haematologica
Journal of the Ferrata Storti Foundation

Early cytokine and chemokine signals shape the anti-AML activity of bispecific engager-secreting T cells

by Natalie J. Holl, Adam Fearnow, Ilias Christodoulou, Stamatia C. Vorri, Ruyan Rahnama, Jun Choe, Alokesh Ghosal, Weng-Ian Ng, Vinay Vyas, Hannah W. Song, Ravi Varadhan and Challice L. Bonifant

Received: March 31, 2025.
Accepted: August 29, 2025.

Citation: Natalie J. Holl, Adam Fearnow, Ilias Christodoulou, Stamatia C. Vorri, Ruyan Rahnama, Jun Choe, Alokesh Ghosal, Weng-Ian Ng, Vinay Vyas, Hannah W. Song, Ravi Varadhan and Challice L. Bonifant. Early cytokine and chemokine signals shape the anti-AML activity of bispecific engager-secreting T cells. Haematologica. 2025 Sept 11. doi: 10.3324/haematol.2025.287934 [Epub ahead of print]

Early cytokine and chemokine signals shape the anti-AML activity of bispecific engager-secreting T cells

Natalie J. Holl,[1] Adam Fearnow,[1] Ilias Christodoulou,[1] Stamatia C. Vorri,[1] Ruyan Rahnama,[1] Jun Choe,[1] Alokesh Ghosal,[2] Weng-Ian Ng,[2] Vinay Vyas,[2] Hannah W. Song,[3] Ravi Varadhan,[1] and Challice L. Bonifant[1]

[1]Department of Oncology, Sidney Kimmel Comprehensive Cancer Center, Johns Hopkins University School of Medicine, Baltimore, MD, USA; [2]Biopharmaceutical Development Program, Frederick National Laboratory for Cancer Research, Leidos Biomedical Research, Inc, Frederick, MD, USA; [3]Center for Cellular Engineering, Department of Transfusion Medicine, National Institutes of Health, Bethesda, MD, USA

Short title: T-cell pre-selection improves ENG-T cell activity

Correspondence should be addressed to C.L.B.
Challice L. Bonifant, MD, PhD
1650 Orleans Street
Baltimore, MD 21287
Email: cbonifa2@jh.edu

Data sharing statement:
All data are available from the corresponding author upon request. Raw and gene counts from bulk RNAseq data generated for this study can be found in the National Center for Biotechnology Information Gene Expression Omnibus (accession number GSE277096, reviewer access token: qrobcewuxngvxgh).

Acknowledgements
We thank Stephen Gottschalk, St. Jude Children's Research Hospital, for advice and review of the data presented in this manuscript and Ada Tam from the SKCCC High Parameter Flow Core for assistance with selected flow cytometry experiments. We also thank Worod Allak and Tricia Nilles from the Bloomberg Flow Cytometry and Immunology Core for technical assistance with our Luminex assay.

Funding
This research was funded in part by NCI Contract No. HHSN26120150003I/HHSN26100077, and an ALSF Million Mile Award (C.L.B.). N.J.H. and J.C. are PhD candidates at Johns Hopkins University. This work is submitted in partial fulfillment of the requirement for the PhD.

Authorship contributions
Contribution: N.J.H. conceptualization, formal analysis, investigation, methodology, visualization, writing – original draft, writing – review & editing; A.F. investigation, writing – review & editing; I.C. investigation, writing – review & editing; S.C.V. investigation, writing – review & editing; R.R. investigation, writing – review & editing; J.C. investigation, writing – review & editing; A.G. resources, writing – review & editing; W.N. resources, writing – review & editing; V.V. resources, writing – review & editing; H.W.S. conceptualization, writing – review & editing; R.V. formal analysis, writing – review & editing; C.L.B. conceptualization, formal analysis, funding acquisition, project administration, methodology, supervision, writing – review & editing.

Conflict-of-interest disclosure
C.L.B. has been awarded and has pending patent applications describing the use of engineered T and NK cells as therapeutics. C.L.B. has received research support from Merck, Sharp, and Dohme, Inc, Bristol-Myers

Squibb, and Kiadis, Pharma. N.J.H has pending patent applications describing the use of engineered NK cells as therapeutics.

Keywords:
Engineered T cells, bispecific engager, pre-selection, manufacturing environment, clinical manufacturing

Abstract

Immunotherapies, including cell therapies, are effective anti-cancer agents. However, cellular product persistence can be limiting with short functional duration of activity contributing to disease relapse. A variety of manufacturing protocols are used to generate therapeutic engineered T-cells; these differ in techniques used for T-cell isolation, activation, genetic modification, and other methodology. We sought to determine how pre-selection affected the phenotype of T cells engineered to secrete a CD123xCD3 bispecific engager (ENG-T). These cells were designed to treat acute myeloid leukemia (AML). We evaluated the effect of T-cell selection on transduction efficiency, T-cell activation, short- and long-term anti-AML cytotoxicity, and gene transcription. Unselected, CD4, CD8, and CD4/CD8 pre-selected ENG-T cells have minor differences in T-cell subset components, equivalent activation, and equal cytotoxicity in short-term assays. While unselected and CD4/CD8-selected ENG-T cells have identical CD4:CD8 composition prior to target cell exposure, serial stimulation *in vitro* showed CD4/CD8 pre-selection supports ENG-T cell survival and long-term activity. Likewise, CD4 and CD4/CD8 pre-selected ENG-T cells display superior anti-tumor efficacy and prolong murine survival in AML xenografts. Unselected ENG-T cells are exposed to cytokines during early manufacture that imprint upregulation of intracellular inflammatory pathways. This early activation likely underpins long-term observed functional differences. Pre-selection of T cells from banked patient biospecimens decreased blast contamination, exposure to inflammatory cytokines, and may improve T-cell expansion during manufacture. Pre-selection of T-cell products should continue to be performed to enhance the quality of clinical cellular therapeutics.

Introduction

The use of chimeric antigen receptor (CAR) T cell therapy has dramatically improved outcomes for patients with relapsed and refractory B-cell malignancies.[1] However, clinical trial meta-analysis and long-term follow-up of patients treated with CAR-T cells has revealed high relapse rates.[1-3] There remain unknown factors that contribute to therapy failure. Manufacturing methods determine cell therapy phenotype,[4,5] yet, there is a lack of manufacturing standardization across CAR-T cell products, even those that target the same antigen for the same indication. Expansion of CAR-T cell products has been reported directly from whole peripheral blood mononuclear cells (PBMCs) using plate-bound anti-CD3 and anti-CD28 antibodies and a mixture of IL-7 and IL-15.[6-8] Others use alternative manufacturing strategies, with the use of CD3/CD28-stimulating microbeads and IL-2 support being common.[9-11]

Selection of CD4+ and CD8+ cells from whole PBMCs using magnetic isolation before activation and expansion is an additional step incorporated by some groups, with the goal of either setting a consistent ratio of CD4:CD8 cells[12] or to remove contaminating blasts that survive T-cell expansion.[13] CAR-T cells with a defined CD4:CD8 ratio have demonstrated improved anti-tumor efficacy in preclinical models[10,14] and are extremely potent in patients with B-cell acute lymphoblastic leukemia.[12] Selection of CD4+ and CD8+ cells before activation also allowed for anti-CD22 CAR-T cell doses to be decreased in clinical trial.[5] T-cell selection steps are costly and add complexity to already complicated manufacturing protocols,[15] limiting their widespread adoption. Manufacturing standards can differ even within the same institution. For example, some trials at the University of Pennsylvania include a selection step prior to cell plating and transduction,[16,17] while others expand cells directly from whole PBMCs.[11,18,19] To date, seven engineered T-cell therapies have been approved for clinical use.[13,20-30] Of these products, only three (brexucabtagene autoleucel, lisocabtagene maraleucel, and ciltacabtagene autoleucel) assert selection steps. Activation and transduction methodology also differ, as summarized in **Supplemental Table 1**.

These differences present challenges for those developing manufacturing platforms for novel engineered T-cell therapies. There is clearly a lack of consensus regarding which activation method is superior and if the benefits of selection can balance increased manufacturing complexity. While selecting CD4+ and CD8+ cells has been shown to modulate CAR-T anti-tumor efficacy,[5,31] the direct impact of selection on the molecular characteristics

of engineered T cells has not been thoroughly examined. Defining these characteristics may help identify best manufacturing practices to improve engineered T-cell products in general.

CAR-T cells have yet to show optimal efficacy against acute myeloid leukemia (AML). It has been demonstrated that myeloid cells[32,33] and AML blasts can impair effective T-cell expansion.[34] These challenges, as well as a lack of an ideal tumor target, have together contributed to the observed poor response to immunotherapies in patients diagnosed with AML. Our lab has developed a T-cell therapy (ENG-T) engineered to secrete a bispecific T-cell engager molecule that targets CD123 (CD123xCD3), an AML associated antigen.[35-38] T cells engineered to secrete an engager have high therapeutic potential as the protein can bind and functionalize both engineered and unmodified T cells. Infused cells can also recruit and activate any cells in the patient T-cell reservoir, amplifying anti-tumor effect.

To translate our anti-AML T-cell therapy, we questioned if pre-selection was necessary for manufacture, which populations to select, and how selection before activation affected our final product. The heterogeneity of AML complicates manufacture from autologous blood cells, as AML blasts can express CD4,[39] potentially leading to blast selection and contamination. While CD4+ CAR-T cells have been shown critical for CAR-T cell persistence and tumor control,[10] their necessity has not been established for ENG-T cells. We evaluated the impact of positive selection on ENG-T cell phenotype and function. We compared ENG-T cells produced from CD4, CD8, and CD4/CD8-selected starting material to those expanded directly from whole PBMCs and found equivalent activity, equal cytotoxicity, and similar immunophenotype in short-term studies. Differences emerged in the treatment responses in AML xenografts, which were further examined in long-term in vitro assays in unselected and CD4/CD8 pre-selected ENG-T cells. CD4/CD8-selected ENG-T cells were exposed to fewer inflammatory cytokines during early manufacture. Pre-selected ENG-T cells also displayed improved expansion and survival during serial stimulation with AML *in vitro*. The manufacturing environment of unselected ENG-T cells contributed to alterations in gene transcription that correlated with lesser performance *in vivo*. To further validate our manufacturing plan for future clinical studies, we engineered ENG-T cells from unselected and CD4/CD8-selected biospecimens from five AML patients. Selection decreased blast contamination, decreased concentrations of inflammatory cytokines early in manufacture, and has the potential to improve T-cell product expansion.

Methods

Flow cytometry, cell line maintenance, CD123xCD3 transgene generation, viral production, ENG-T cell production, transduction efficiency, short term cytotoxicity measurement, mouse modeling, murine blood processing, and RNA sequencing were performed using standard protocols, detailed in **Supplementary Methods** including a table of antibodies used (**Table S2**). All research using primary human cells was approved or acknowledged by the Johns Hopkins University School of Medicine Institutional Review Board.

CD123xCD3 quantification

CD123xCD3 concentration was quantified by ELISA as described.[35] Concentrations were assessed in the growth media of patient-derived ENG-T cells on day 7 or day 10, after 1:1 patient-derived ENG-T cell co-culture with autologous AML, and in media collected 24h after plating healthy donor ENG-T cells in complete RPMI supplemented with rhIL-7 and rhIL-15. A 96-well plate was coated with 20ng recombinant human CD123 (rhCD123, Sino Biological) per well. A standard curve was prepared using recombinant CD123xCD3 (Creative Biolabs) with samples and standards incubated in duplicate. Absorbance was recorded at 450nm and 570nm using a BMG CLARIOstar Plus microplate reader. Standard curves and concentrations were calculated using Microsoft Excel Version 16.94.

Cytokine quantification

Healthy donor ENG-T cells were incubated for 24h 1:1 with CD123+ cell lines (MOLM-13, MV-4-11, and K-562.CD123, **Figure S1A**) and CD123-negative (K-562) in complete RPMI. IL-2 and IFN-γ were quantified in the media of these co-cultures. IL-1β, IL-6, and CXCL10 were quantified in the expansion media of patient-derived ENG-T cells. All proteins were quantified using DuoSet ELISA kits (R&D Systems) according to the manufacturer's instructions. Absorbance was recorded at 450nm and 570nm. Microsoft Excel Version 16.94 was used for calculations. During healthy donor-derived ENG.NLSmCh-T cell manufacture and serial stimulation, media was collected and stored. Samples were assayed using a 29-analyte Human Magnetic Luminex Assay Luminex kit (R&D Systems) according to the manufacturer's instructions. One analyte was removed from analysis due to elevated blank fluorescent intensity. Samples were run in duplicate with a Luminex MagPix by the Johns Hopkins Bloomberg Flow Cytometry and Immunology Core. Data were analyzed using BioPlex Manager 6.1.1.

Serial stimulation

Unselected and pre-selected T cells engineered with ENG.NLSmCh were plated 1:1 with MOLM-13 engineered to express nuclear localized enhanced green fluorescent protein (MOLM-13.NLSGFP) in poly-D-lysine-coated 96-well plates (Corning). Cells were tracked with an Incucyte S3 live cell imaging system. ENG.NLSmCh-T cells were stimulated by adding 1e5 MOLM-13.NLSGFP every 48h for healthy donor cells and every 72h for patient-derived cells. Images were collected every 4h over 10-22 days. Data were accumulated in the Incucyte 2021A or 2022B Rev2 software. Raw data were analyzed in Microsoft Excel Version 16.94.

Statistical analysis

Statistical analyses were performed in GraphPad Prism 10 unless otherwise noted. Statistical methods used are specified in figure captions. Compositional analyses were performed using the R package DirichletReg[40,41] and Dirichlet regression models with common parametrization. The eulerr R package[42] was used to generate Euler diagrams using version R-4.4.1 and RStudio v2024.04.2+764.

Results

Transduction and expression of CD123xCD3 are equivalent regardless of T-cell pre-selection

T-cell subsets were selected using magnetic column isolation (**Figure 1A**). CD4+ and CD8+ selections of healthy donor PBMCs yielded pure T-cell products of the desired populations (**Figure S1B-C**). Cells were transduced with a retroviral vector encoding both the CD123xCD3 sequence and full length CD20 two days after activation (**Figure 1B**). Stable purity was confirmed with low contamination detected on day 7 after isolation (**Figure 1C**). Notably, unselected and CD4/CD8 pre-selected ENG-T cells had equivalent proportions of CD4+, CD8+, double positive (+/+) and double negative (-/-) T cells on day 7. Transduction with resultant CD123xCD3 secretion did not alter the distribution of CD4+, CD8+, +/+, or -/- cells, with the exception of CD8-selected ENG-T cells which were enriched for +/+ cells (**Figure 1C**). To test whether our selection process altered transduction or expression, we assessed CD20 surface expression by flow cytometry (**Figure 1D**) and quantified CD123xCD3 protein secretion by ELISA (**Figure 1E**). There were no differences in transduction efficiency or in CD123xCD3 production between conditions.

Short-term in vitro functionality of ENG-T cells is equal across selection groups

The T-cell subset composition of ENG-T cells was measured after one week of *ex vivo* expansion to define percentages of naïve/stem central memory (naïve/SCM), central memory (CM), effector memory (EM), and T effector (Teff) cells. There were minor differences in subset distribution between selection groups (**Figure 2A**). CD4+ unselected ENG-T distributions differed from CD4 pre-selected and CD4+ CD4/CD8 pre-selected ENG-T, with differences driven by increased naïve/SCM and CM proportions in unselected cells. CD8+ unselected ENG-T distributions differed from CD8 pre-selected ENG-T, with differences driven by increased naïve/SCM and Teff components of unselected cells. In general, transduction did not cause compositional differences, except in unselected cells, which had alterations driven by increased CM percentages in both CD4+ and CD8+ ENG-T populations (**Figure 2A**). Target-specific T-cell activation was tested using CD123+ and negative cell lines. ENG-T cells co-cultured with CD123+ targets produced similar amounts of IL-2 and, in most cases, IFNγ regardless of pre-selection (**Figure 2B**). Selection did not impact the ability of ENG-T cells to kill targets (**Figure 2C**). All ENG-T cells killed CD123+ targets more effectively than unmodified cells without variability between selection groups at each tested effector-to-target ratio. As previously reported,[35,36] ENG-T cells were not cytotoxic against a CD123-negative cell line, confirming antigen-specificity. When ENG-T cells were titrated such that the secreted CD123xCD3 was below our detection threshold, specific cytotoxicity of CD4/CD8 pre-selected ENG-T cells was not affected (**Figure S2**). In sum, CD123xCD3 secretion potently increases T-cell antigen-specific cytotoxicity, regardless of pre-selection.

CD4 and CD4/CD8 pre-selection improve ENG-T cell tumor control in vivo

All *in vitro* studies indicated selection did not alter engineered T-cell functionality. We were hopeful that CD8-selected ENG-T cells would sufficiently eliminate leukemia *in vivo* while mitigating the possibility of CD4+ leukemia contamination during manufacture. To test if CD8 pre-selected ENG-T cells retain *in vivo* activity, we injected NSG mice with a CD123+ AML cell line expressing ffLuc, monitored leukemia engraftment, then treated mice 7 days later with unmodified T cells or ENG-T cells manufactured from healthy unselected PBMC, CD4+, CD8+, or CD4+/CD8+ starting material (**Figure 3A**). Animals were monitored over the course of 100 days with weekly imaging and peripheral blood collection (**Figures 3B-C**). All mice treated with ENG-T cells had tumor control and prolonged survival compared to those who received unmodified cells (**Figure 3D**). Mice

treated with CD4 and CD4/CD8 pre-selected ENG-T cells had a survival advantage compared to animals injected with unselected or CD8 pre-selected ENG-T cells (**Figure 3D**). Mice treated with CD4 pre-selected ENG-T cells were cured and thriving at the experimental endpoint. The prolonged survival of mice that received ENG-T produced from CD4+ starting material was associated with a trend toward increased circulating ENG-T cells, but low sample numbers precluded a sufficiently powered analysis (**Figure 3E**). Notably, despite the marked difference in *in vivo* anti-tumor activity of unselected and CD4/CD8 pre-selected ENG-T cells, at the time of treatment these two ENG-T cell products had the same percentages of CD4+ and CD8+ cells (**Figure 1D**) as well as similar subset compositions (**Figure 2A**). We further studied our products to identify determinants of the observed *in vivo* differences between unselected and CD4/CD8 pre-selected ENG-T cells.

Serial stimulation of ENG-T cells uncovers requirement for CD4+ and CD8+ ENG-T cells

To study the contribution of individual CD4+ versus CD8+ cells to differential *in vivo anti*-tumor activity, we designed an *in vitro* serial stimulation assay. ENG-T cells engineered to express nuclear localized (NL) mCherry (ENG.NLSmCh, **Figure S3**) were plated in co-culture with CD123+ MOLM-13 cells engineered with NL green fluorescent protein (MOLM-13.NLSGFP[43], **Figure S4A**). AML and ENG-T cells were individually tracked by measurement of GFP and mCherry fluorescence (**Figure 4A**). To elucidate the relative contribution of CD4+ and CD8+ ENG-T cells to directed cytotoxicity and T-cell survival, ENG-T cell products with discrete CD4:CD8 ratios (CD4+ only, 3:1, 1:1, 1:3, CD8+ only) were tested. Comparison of fixed ratios of CD4:CD8 ENG-T cells reinforce the need for both cell populations for sustained target cell killing. All ENG-T cell products containing both CD4 and CD8 cells chronically stimulated with AML had the potential to maintain robust cytotoxicity for several stimulations regardless of CD4+ starting percentage. Curve fitting of the data highlights that CD4+ and CD8+ alone ENG-T products demonstrate progressively diminished killing capacity beginning at the third and fifth stimulations, respectively, with complete lack of killing by the CD8+ only product by stimulation 8 (**Figure S4B, Table S3**). Increasing ratios of CD4:CD8 cells supported durability of target cell killing with 3:1>1:1>1:3 by stimulations 10 and 11 (**Figure 4A, S4B**). Measurement of T-cell numbers verified the increased capacity of CD4+ cells for more robust expansion and sustained persistence, with increasing CD4:CD8 ratio correlating with degree of T-cell proliferation and survival (**Figure 4A-B**). Interestingly, T cells

sampled at experiment end (D22) had converted to a majority CD8+ population in all conditions save the CD4+ alone product (**Figure 4C**). The relatively poorer cytotoxic activity and ENG-T cell expansion of unselected ENG-T cells seen in the xenograft model was replicated when direct comparison of unselected ENG-T cell products to the most relevant CD4:CD8 ratios for each T-cell donor was performed (**4D-E, Figure S4C-D**). Given the clear necessity for both CD4+ and CD8+ ENG-T cells for sustained anti-AML cytotoxicity, we further limited our investigation to dual CD4/CD8-selected products as compared to unselected. To minimize cell manipulation, we decided together with our clinical manufacturing team to perform combined CD4/CD8 selection to avoid the need for two separate selection steps.

Neither ENG-T cell subset distribution nor exhaustion marker expression define the dysfunctional ENG-T cell phenotype

To investigate the reason for inferior unselected T-cell expansion, we first investigated whether serial stimulation led to selective loss of memory-like T-cell subsets, which have been associated with CAR-T cell clinical durability.[44,45] We noted a shift in subset distributions on day 7 before co-culture driven by differences in the Teff percentage in both CD4+ and CD8+ populations (**Figure 5A and S5A**); however, these minimal differences were not apparent after 5 repeat serial stimulations with target cells (**Figure 5A and S5B**). We next evaluated T cells post-chronic target exposure for markers of exhaustion (PD-1, TIM-3, and LAG-3). We did not identify differences in individual or co-expressed exhaustion markers between unselected and CD4/CD8 pre-selected ENG-T cells (**Figures 5B, S5C-D**).

Unselected T cells are exposed to an inflammatory manufacturing environment

Given the lack of differences in T-cell composition or exhaustion, we hypothesized that immunosuppressive cells present in unselected starting material may be negatively imprinting T cells during manufacture.[32] To test for the presence of immunomodulatory molecules, we collected supernatant during manufacture and serial stimulation of unselected and CD4/CD8 pre-selected ENG-T cells. Strikingly, during initial manufacturing (days 1 and 2) we measured increased levels of pro-inflammatory cytokines and chemokines in the media of unselected cells (**Figure 5C**). We detected increased levels of CCL2, CCL3, CXCL10, IL-1α, IL-1β, IL-6, IL-1 receptor antagonist (IL-1RA), and IL-6Rα. There were no differences in IL-10 concentrations, suggesting that Tregs were likely not differentially activated or selected. By day 7 of T-cell expansion, inflammatory mediator

differences had resolved (**Figure S6**). We similarly found no differences during or after serial target stimulation (**Figures 5C and S6**).

Unselected T cells upregulate activation and inflammatory markers during manufacture

To further understand the observed differences in T-cell survival and *in vivo* anti-tumor activity, bulk RNA sequencing was performed on unselected and CD4/CD8 pre-selected ENG-T cells. Overall gene expression did not vary between the two groups (**Figure S7A**); yet, unbiased clustering analysis clustered CD4/CD8 pre-selected separately from unselected ENG-T cells, highlighting global transcriptional differences (**Figures 6A-B and S7B**). Of transcripts with significant differences, 203 genes were upregulated and 99 downregulated in CD4/CD8 pre-selected ENG-T cells compared to unselected ENG-T cells (**Figure 6C**). Further analysis included using Enrichr[46,47] on these clustered gene sets with pathway enrichment compared to the Reactome 2022 database (**Tables S4 and S5**) and gene ontologies examined against GO Biological Process 2023 (**Tables S6 and S7**). Relevant reactome and GO terms identified that unselected ENG-T cells dowregulate genes associated with metabolism, ion homeostasis, and several important cell signaling regulatory pathways, including WNT and NOTCH, as well as anti-apoptosis mediators (**Figure 6D**). Additionally, regulators of TCR signaling were downregulated in unselected ENG-T cells. Upregulated transcripts in unselected ENG-T cells are associated with cell cycle, cytokine signaling, chemokine signaling, and effector function (**Figure 6D**).

Pre-selection of patient-derived ENG-T cells improves product characteristics

To further validate our clinical manufacturing plan, we engineered ENG.NLSmCh-T cells from unselected and CD4/CD8 pre-selected biospecimens collected from the peripheral blood of three patients diagnosed with CD123+ AML (5800, 6034, and 6675, **Table S8**). CD4/CD8 pre-selection prior to T-cell activation decreased CD3-negative contamination of all patient samples (**Figure 7A**) prior to transduction. Products were successfully modified (**Figure 7B**) with contamination further reduced after *ex vivo* expansion post-activation in sample 5800 and 6034, both of which had low level (5800) or no (6034) disease contamination prior to T-cell activation (**Figure 7C**). We also tested isolation of two bone marrow-derived patient biospecimens (4293 and 4316), with similar outcome (**Figure S8A-B**). Non-T cell contamination was reduced by pre-selection, and all samples were satisfactorily transduced (**Figure S8C**). ENG-T cells from patients 6675 and 4316 ultimately failed to expand to a number needed for further functional analysis, likely due to disease contamination

(**Figures 7D, S8D-E**). Despite failed expansion and relatively low transduction efficiencies, all evaluable ENG.NLSmCh products produced quantifiable secreted CD123xCD3 (**Figure 7E, S8F**). The media of unselected ENG-T cells from patients 6034, 5800, and 4293 had increased concentrations of IL-1β, IL-6, and CXCL10 measured on the day following plating (**Figures 7F, S8G**). Patient derived ENG.NLSmCh-T cells with sufficient expansion were serially stimulated with MOLM-13.NLSGFP (**Figure S9A**). Unselected ENG-T cells from patient 4293 killed over three AML-stimulations, while CD4/CD8-selected cells effectively killed AML across two stimulations. CD4/CD8 pre-selected ENG-T cells again had increased expansion when challenged with target cells when compared to matched unselected cells (**Figure S9A**). ENG-T cells co-cultured with autologous AML were cytotoxic to CD33+ blasts (**Figure S9B-C**). CD123xCD3 was detectable in the media of ENG-T cells co-cultured with autologous AML (**Figure S9D**).

Discussion

We began this study to develop the clinical manufacturing standard for an ENG-T cell product and to elucidate the biological effects of pre-selection. While we did not observe differences in T-cell activation or antigen-specific cytotoxicity, and only minor differences in the subset composition of ENG-T cells manufactured from unselected, CD4, CD8, or CD4/CD8 pre-selected starting material in short-term assays, mice with AML xenografts treated with CD4 or CD4/CD8 pre-selected ENG-T cells had improved survival. CD4+ ENG-T cell support was required for optimal anti-tumor efficacy, as has been demonstrated using CAR-T cells.[10] Overall improved survival of mice treated with CD4/CD8 pre-selected as compared to unselected ENG-T cells could not be readily explained; while unselected ENG-T cells appeared to have a higher percentage of naïve and central memory subsets which have been associated with greater expansion, persistence, and anti-tumor efficacy of engineered T-cells in the clinic,[44,45] CD4/CD8 pre-selected ENG-T cells had superior tumor control. Our identified optimal ENG-T cell product for use as therapy for murine AML xenografts would be one manufactured from selected CD4+ starting material. However, we recognize that exclusive CD4+ selection may result in blast contamination, the seriousness of which was highlighted by a prior study that identified transduction of a single leukemic clone during CAR-T cell manufacturing with conferred resistance that ultimately led to disease relapse.[48] Our upcoming clinical trial testing CD123-ENG T cells includes release

criteria and intensive clinical monitoring to evaluate for infusion and emergence of transduced non-T cells. In addition, we acknowledge the immense body of data that clearly identifies the need for CD8+ cells as anti-tumor effectors,[49,50] supported by our extended *in vitro* study of sustained anti-tumor activity. We are also cognizant of the inherent physiological and environmental differences when using immunodeficient mice that limit the generalization of data obtained exclusively using animal models.

Our *in vivo* study illuminated a puzzling difference between unselected and CD4/CD8 pre-selected ENG-T cells. Despite near apparent identical T-cell characteristics at the time of treatment, CD4/8 pre-selected ENG-T cells had improved anti-tumor activity. Further analyses revealed greater expansion and subsequent prolonged persistence of CD4/CD8-selected ENG-T cells when challenged by chronic stimulation *in vitro*. We observe increased T-cell numbers to be biologically relevant with alignment to the durability of anti-tumor activity *in vivo*.

Detailed testing of the ENG-T manufacturing environment highlighted differences dependent on pre-selection of T cells. We detected higher levels of mediators that influence T-cell differentiation, recruitment, and anti-cancer potential: CCL2, CCL3, CXCL10, IL-1α, IL-1β, IL-6, IL-1RA, and IL-6Rα.[51-66] Given that many of the analytes that were detected at increased levels in the media of unselected cells are known to be secreted by myeloid cells, we conclude that these non-T cells imprint a dysfunctional phenotype on the ENG-T product. Although T cells are still able to effectively expand with myeloid cell contamination,[32,33] any myeloid presence is potentially detrimental if sufficient immunomodulatory factor secretion occurs. Though less likely, we recognize that unselected ENG-T cells may have also been influenced by γδ T cells as these cells do not bind to anti-CD4 or anti-CD8 microbeads.[31]

Overall, transcriptional analysis revealed phenotypic differences between ENG-T manufactured from whole PBMC or CD4+/CD8+ starting material. Unselected cells displayed higher levels of transcripts associated with inflammation and proliferation in the absence of AML targets. For example, ITGAM, FUT7, TRPC3, CD80, and CD40LG have all been detected in T cells following activation[67-72] and these were all upregulated in unselected ENG-T cells. Interestingly, upregulation of RGS16 was also detected, a gene that has been linked to anti-tumor CD8+ T-cell exhaustion.[73] Generally higher, unspecific basal activation may explain why unselected ENG-T cells were less effective over the long-term in our serial stimulation assays and *in vivo* AML xenograft study.

Reduced immunomodulatory cytokine exposure during manufacturing is associated with transcriptional expression that may prepare CD4/CD8 pre-selected ENG-T cells for the metabolic demands of expansion and differentiation. CD4/CD8 pre-selected ENG-T cells upregulated transcripts associated with ionic transport and homeostasis, including calcium (RYR1, NOL3, CACNA1I, JPH2, PLCH2, CACNA1F) and sodium (FXYD7, FGF11). Important biosynthetic metabolic pathways were upregulated in pre-selected ENG-T cells. For example, the oxidation and synthesis of fatty acids is required for T-cell differentiation and memory,[74] and genes involved in this process (GSTM2, EPHX1, DPEP2) were upregulated. Important regulators of TCR signaling and T-cell cytotoxicity were also upregulated in CD4/CD8 pre-selected ENG-T cells. PIK3IP1 negatively regulates TCR signaling by inhibition of PI3K,[75] with higher expression likely preventing acquisition of an overactive phenotype. EBF4 positively regulates genes involved in T-cell cytotoxicity, including granzymes and perforin, with transcription repression after T-cell stimulation.[76] Decreased EBF4 transcript levels in unselected ENG-T cells is further evidence of unproductive, non-specific activation during manufacturing. Taken together with the pro-inflammatory factors detected in the manufacturing environment, unselected T cells are conditioned to be more highly activated before target exposure and are likely to exhaust sooner than CD4/CD8-selected ENG-T cells.

We produced ENG-T cells from available primary AML patient peripheral blood and bone marrow biospecimens. CD4/CD8 pre-selection led to higher sustained cell numbers during serial stimulation. Importantly, two products failed to expand or survive *ex vivo* due to high leukemic contamination, readily detectable via flow cytometric analysis. Of products that did expand, both selected and unselected cells were engineered and secreted CD123xCD3 ENG protein. As anticipated, patient-derived ENG-T cells were less active and expanded less well than healthy donor-derived ENG-T cells overall, likely because of pre-existing AML-directed T-cell suppression by malignant blasts.

In summary, we found that positive selection of CD4+/CD8+ cell populations prior to manufacture produces superior ENG-T cells. Mechanistically, unselected T cells are phenotypically imprinted by immunosuppressive cells early in *ex vivo* manufacture, altering their transcriptional profile and underpinning long-term effector cell behavior. The manufacturing environment of T-cell products is highly influential and curation via selection of

desired cell populations can ensure the long-term health of T cells used as immunotherapy for devastating diseases.

References

1. Cappell KM, Kochenderfer JN. Long-term outcomes following CAR T cell therapy: what we know so far. Nat Rev Clin Oncol. 2023;20(6):359-371.

2. Shah NN, Lee DW, Yates B, et al. Long-Term Follow-Up of CD19-CAR T-Cell Therapy in Children and Young Adults With B-ALL. J Clin Oncol. 2021;39(15):1650-1659.

3. Zinzi A, Gaio M, Liguori V, et al. Late relapse after CAR-T cell therapy for adult patients with hematologic malignancies: A definite evidence from systematic review and meta-analysis on individual data. Pharmacol Res. 2023;190:106742.

4. Ceppi F, Wilson AL, Annesley C, et al. Modified Manufacturing Process Modulates CD19CAR T-cell Engraftment Fitness and Leukemia-Free Survival in Pediatric and Young Adult Subjects. Cancer Immunol Res. 2022;10(7):856-870.

5. Shah NN, Highfill SL, Shalabi H, et al. CD4/CD8 T-Cell Selection Affects Chimeric Antigen Receptor (CAR) T-Cell Potency and Toxicity: Updated Results From a Phase I Anti-CD22 CAR T-Cell Trial. J Clin Oncol. 2020;38(17):1938-1950.

6. Hill LC, Rouce RH, Wu MJ, et al. Antitumor efficacy and safety of unedited autologous CD5.CAR T cells in relapsed/refractory mature T-cell lymphomas. Blood. 2024;143(13):1231-1241.

7. Ramos CA, Grover NS, Beaven AW, et al. Anti-CD30 CAR-T Cell Therapy in Relapsed and Refractory Hodgkin Lymphoma. J Clin Oncol. 2020;38(32):3794-3804.

8. Ramos CA, Rouce R, Robertson CS, et al. In Vivo Fate and Activity of Second- versus Third-Generation CD19-Specific CAR-T Cells in B Cell Non-Hodgkin's Lymphomas. Mol Ther. 2018;26(12):2727-2737.

9. Hollyman D, Stefanski J, Przybylowski M, et al. Manufacturing validation of biologically functional T cells targeted to CD19 antigen for autologous adoptive cell therapy. J Immunother. 2009;32(2):169-180.

10. Sommermeyer D, Hudecek M, Kosasih PL, et al. Chimeric antigen receptor-modified T cells derived from defined CD8+ and CD4+ subsets confer superior antitumor reactivity in vivo. Leukemia. 2016;30(2):492-500.

11. Cohen AD, Garfall AL, Stadtmauer EA, et al. B cell maturation antigen-specific CAR T cells are clinically active in multiple myeloma. J Clin Invest. 2019;129(6):2210-2221.

12. Turtle CJ, Hanafi LA, Berger C, et al. CD19 CAR-T cells of defined CD4+:CD8+ composition in adult B cell ALL patients. J Clin Invest. 2016;126(6):2123-2138.

13. Mian A, Hill BT. Brexucabtagene autoleucel for the treatment of relapsed/refractory mantle cell lymphoma. Expert Opin Biol Ther. 2021;21(4):435-441.

14. Riddell SR, Sommermeyer D, Berger C, et al. Adoptive therapy with chimeric antigen receptor-modified T cells of defined subset composition. Cancer J. 2014;20(2):141-144.

15. Song HW, Somerville RP, Stroncek DF, Highfill SL. Scaling up and scaling out: Advances and challenges in manufacturing engineered T cell therapies. Int Rev Immunol. 2022;41(6):638-648.

16. Singh N, Frey NV, Engels B, et al. Antigen-independent activation enhances the efficacy of 4-1BB-costimulated CD22 CAR T cells. Nat Med. 2021;27(5):842-850.

17. Bagley SJ, Logun M, Fraietta JA, et al. Intrathecal bivalent CAR T cells targeting EGFR and IL13Ralpha2 in recurrent glioblastoma: phase 1 trial interim results. Nat Med. 2024;30(5):1320-1329.

18. Maude SL, Frey N, Shaw PA, et al. Chimeric antigen receptor T cells for sustained remissions in leukemia. N Engl J Med. 2014;371(16):1507-1517.

19. Narayan V, Barber-Rotenberg JS, Jung IY, et al. PSMA-targeting TGFbeta-insensitive armored CAR T cells in metastatic castration-resistant prostate cancer: a phase 1 trial. Nat Med. 2022;28(4):724-734.

20. U.S. Food and Drug Administration. KYMRIAH: Package Insert and Medication Guide - KYMRIAH. Updated 07/02/2025. Available from: https://www.fda.gov/vaccines-blood-biologics/cellular-gene-therapy-products/kymriah. Accessed on 2025, Aug 20

21. U.S. Food and Drug Administration. YESCARTA: Package Insert and Medication Guide - YESCARTA. Updated 06/30/2025.. Available from: https://www.fda.gov/vaccines-blood-biologics/cellular-gene-therapy-products/yescarta. Accessed on 2023, Aug 8.

22. U.S. Food and Drug Administration. TECARTUS: Package Insert and Medication Guide - TECARTUS. Updated 06/30/2025. Available from: https://www.fda.gov/vaccines-blood-biologics/cellular-gene-therapy-products/tecartus. Accessed on 2025, Aug 20

23. U.S. Food and Drug Administration. ABECMA (idecabtagene vicleucel): Package Insert and Medication Guide - ABECMA. Updated 06/27/2025. Available from: https://www.fda.gov/vaccines-blood-biologics/abecma-idecabtagene-vicleucel. Accessed on 2025, Aug 20.

24. Friedman KM, Garrett TE, Evans JW, et al. Effective Targeting of Multiple B-Cell Maturation Antigen-Expressing Hematological Malignances by Anti-B-Cell Maturation Antigen Chimeric Antigen Receptor T Cells. Hum Gene Ther. 2018;29(5):585-601.

25. U.S. Food and Drug Administration. BREYANZI: Package Insert and Medication Guide - BREYANZI. Updated 07/31/2025. Available from: https://www.fda.gov/vaccines-blood-biologics/cellular-gene-therapy-products/breyanzi. Accessed on 2025, Aug 20.

26. Teoh J, Brown LF. Developing lisocabtagene maraleucel chimeric antigen receptor T-cell manufacturing for improved process, product quality and consistency across CD19(+) hematologic indications. Cytotherapy. 2022;24(9):962-973.

27. U.S. Food and Drug Administration. CARVYKTI: Package Insert and Medication Guide - CARVYKTI. Updated 06/26/2025. Available from: https://www.fda.gov/vaccines-blood-biologics/cellular-gene-therapy-products/carvykti. Accessed on 2025, Aug 20.

28. Xu J, Chen LJ, Yang SS, et al. Exploratory trial of a biepitopic CAR T-targeting B cell maturation antigen in relapsed/refractory multiple myeloma. Proc Natl Acad Sci U S A. 2019;116(19):9543-9551.

29. U.S. Food and Drug Administration. TECELRA: Package Insert - TECELRA. Updated 08/23/2024. Available from: https://www.fda.gov/vaccines-blood-biologics/cellular-gene-therapy-products/tecelra. Accessed on 2025, Aug 20.

30. D'Angelo SP, Araujo DM, Abdul Razak AR, et al. Afamitresgene autoleucel for advanced synovial sarcoma and myxoid round cell liposarcoma (SPEARHEAD-1): an international, open-label, phase 2 trial. Lancet. 2024;403(10435):1460-1471.

31. Song HW, Benzaoui M, Dwivedi A, et al. Manufacture of CD22 CAR T cells following positive versus negative selection results in distinct cytokine secretion profiles and gammadelta T cell output. Mol Ther Methods Clin Dev. 2024;32(1):101171.

32. Stroncek DF, Ren J, Lee DW, et al. Myeloid cells in peripheral blood mononuclear cell concentrates inhibit the expansion of chimeric antigen receptor T cells. Cytotherapy. 2016;18(7):893-901.

33. Wang X, Borquez-Ojeda O, Stefanski J, et al. Depletion of high-content CD14(+) cells from apheresis products is critical for successful transduction and expansion of CAR T cells during large-scale cGMP manufacturing. Mol Ther Methods Clin Dev. 2021;22:377-387.

34. Kenderian SS, June CH, Gill S. Generating and Expanding Autologous Chimeric Antigen Receptor T Cells from Patients with Acute Myeloid Leukemia. Methods Mol Biol. 2017;1633:267-276.

35. Bonifant CL, Szoor A, Torres D, et al. CD123-Engager T Cells as a Novel Immunotherapeutic for Acute Myeloid Leukemia. Mol Ther. 2016;24(9):1615-1626.

36. Zolov SN, Rietberg SP, Bonifant CL. Programmed cell death protein 1 activation preferentially inhibits CD28.CAR-T cells. Cytotherapy. 2018;20(10):1259-1266.

37. Mu-Mosley H, Ostermann L, Muftuoglu M, et al. Transgenic Expression of IL15 Retains CD123-Redirected T Cells in a Less Differentiated State Resulting in Improved Anti-AML Activity in Autologous AML PDX Models. Front Immunol. 2022;13:880108.

38. Vaidya A, Doherty E, Wu X, et al. Improving the anti-acute myeloid leukemia activity of CD123-specific engager T cells by MyD88 and CD40 costimulation. Haematologica. 2023;108(4):1039-1052.

39. Miwa H, Mizutani M, Mahmud N, et al. Biphasic expression of CD4 in acute myelocytic leukemia (AML) cells: AML of monocyte origin and hematopoietic precursor cell origin. Leukemia. 1998;12(1):44-51.

40. Maier MJ. DirichletReg: Dirichlet Regression. R package version 0.7-1. 2021.

41. Maier MJ. DirichletReg: Dirichlet Regression for Compositional Data in R. Research Report Series: WU Vienna University of Economics and Business; 2014.

42. Larsson J, Godfrey AJR, Gustafsson P, Eberly DH, Huber E, Privé F. eulerr: Area-Proportional Euler and Venn Diagrams with Ellipses. R package version 7.0.2. 2024.

43. Vorri SC, Holl NJ, Leeming M, et al. Activation of Cell Intrinsic Signaling in CAR-T cells via a Chimeric IL7R Domain. Cancer Res Commun. 2024;4(9):2359-2373.

44. Singh N, Perazzelli J, Grupp SA, Barrett DM. Early memory phenotypes drive T cell proliferation in patients with pediatric malignancies. Sci Transl Med. 2016;8(320):320ra323.

45. Xu Y, Zhang M, Ramos CA, et al. Closely related T-memory stem cells correlate with in vivo expansion of CAR.CD19-T cells and are preserved by IL-7 and IL-15. Blood. 2014;123(24):3750-3759.

46. Kuleshov MV, Jones MR, Rouillard AD, et al. Enrichr: a comprehensive gene set enrichment analysis web server 2016 update. Nucleic Acids Res. 2016;44(W1):W90-97.

47. Chen EY, Tan CM, Kou Y, et al. Enrichr: interactive and collaborative HTML5 gene list enrichment analysis tool. BMC Bioinformatics. 2013;14:128.

48. Ruella M, Xu J, Barrett DM, et al. Induction of resistance to chimeric antigen receptor T cell therapy by transduction of a single leukemic B cell. Nat Med. 2018;24(10):1499-1503.

49. Galli E, Bellesi S, Pansini I, et al. The CD4/CD8 ratio of infused CD19-CAR-T is a prognostic factor for efficacy and toxicity. Br J Haematol. 2023;203(4):564-570.

50. Raskov H, Orhan A, Christensen JP, Gogenur I. Cytotoxic CD8(+) T cells in cancer and cancer immunotherapy. Br J Cancer. 2021;124(2):359-367.

51. Liu M, Guo S, Stiles JK. The emerging role of CXCL10 in cancer (Review). Oncol Lett. 2011;2(4):583-589.

52. Karin N. CXCR3 Ligands in Cancer and Autoimmunity, Chemoattraction of Effector T Cells, and Beyond. Front Immunol. 2020;11:976.

53. Schaller TH, Batich KA, Suryadevara CM, Desai R, Sampson JH. Chemokines as adjuvants for immunotherapy: implications for immune activation with CCL3. Expert Rev Clin Immunol. 2017;13(11):1049-1060.

54. Castellino F, Huang AY, Altan-Bonnet G, Stoll S, Scheinecker C, Germain RN. Chemokines enhance immunity by guiding naive CD8+ T cells to sites of CD4+ T cell-dendritic cell interaction. Nature. 2006;440(7086):890-895.

55. Trifilo MJ, Bergmann CC, Kuziel WA, Lane TE. CC chemokine ligand 3 (CCL3) regulates CD8(+)-T-cell effector function and migration following viral infection. J Virol. 2003;77(7):4004-4014.

56. Kang TG, Park HJ, Moon J, Lee JH, Ha SJ. Enriching CCL3 in the Tumor Microenvironment Facilitates T cell Responses and Improves the Efficacy of Anti-PD-1 Therapy. Immune Netw. 2021;21(3):e23.

57. Hao Q, Vadgama JV, Wang P. CCL2/CCR2 signaling in cancer pathogenesis. Cell Commun Signal. 2020;18(1):82.

58. Tu MM, Abdel-Hafiz HA, Jones RT, et al. Inhibition of the CCL2 receptor, CCR2, enhances tumor response to immune checkpoint therapy. Commun Biol. 2020;3(1):720.

59. Zhang J, Patel L, Pienta KJ. Targeting chemokine (C-C motif) ligand 2 (CCL2) as an example of translation of cancer molecular biology to the clinic. Prog Mol Biol Transl Sci. 2010;95:31-53.

60. Cavalli G, Colafrancesco S, Emmi G, et al. Interleukin 1alpha: a comprehensive review on the role of IL-1alpha in the pathogenesis and treatment of autoimmune and inflammatory diseases. Autoimmun Rev. 2021;20(3):102763.

61. Van Den Eeckhout B, Tavernier J, Gerlo S. Interleukin-1 as Innate Mediator of T Cell Immunity. Front Immunol. 2020;11:621931.

62. Kiss M, Vande Walle L, Saavedra PHV, et al. IL1beta Promotes Immune Suppression in the Tumor Microenvironment Independent of the Inflammasome and Gasdermin D. Cancer Immunol Res. 2021;9(3):309-323.

63. Dienz O, Rincon M. The effects of IL-6 on CD4 T cell responses. Clin Immunol. 2009;130(1):27-33.

64. Raphael I, Nalawade S, Eagar TN, Forsthuber TG. T cell subsets and their signature cytokines in autoimmune and inflammatory diseases. Cytokine. 2015;74(1):5-17.

65. Arend WP, Malyak M, Guthridge CJ, Gabay C. Interleukin-1 receptor antagonist: role in biology. Annu Rev Immunol. 1998;16:27-55.

66. Gupta M, Stenson M, O'Byrne M, et al. Comprehensive serum cytokine analysis identifies IL-1RA and soluble IL-2Ralpha as predictors of event-free survival in T-cell lymphoma. Ann Oncol. 2016;27(1):165-172.

67. Christensen JE, Andreasen SO, Christensen JP, Thomsen AR. CD11b expression as a marker to distinguish between recently activated effector CD8(+) T cells and memory cells. Int Immunol. 2001;13(4):593-600.

68. Wagers AJ, Waters CM, Stoolman LM, Kansas GS. Interleukin 12 and interleukin 4 control T cell adhesion to endothelial selectins through opposite effects on alpha1, 3-fucosyltransferase VII gene expression. J Exp Med. 1998;188(12):2225-2231.

69. Philipp S, Strauss B, Hirnet D, et al. TRPC3 mediates T-cell receptor-dependent calcium entry in human T-lymphocytes. J Biol Chem. 2003;278(29):26629-26638.

70. Soskic B, Jeffery LE, Kennedy A, et al. CD80 on Human T Cells Is Associated With FoxP3 Expression and Supports Treg Homeostasis. Front Immunol. 2020;11:577655.

71. Rollins MR, Gibbons Johnson RM. CD80 Expressed by CD8(+) T Cells Contributes to PD-L1-Induced Apoptosis of Activated CD8(+) T Cells. J Immunol Res. 2017;2017:7659462.

72. Daoussis D, Andonopoulos AP, Liossis SN. Targeting CD40L: a promising therapeutic approach. Clin Diagn Lab Immunol. 2004;11(4):635-641.

73. Weisshaar N, Wu J, Ming Y, et al. Rgs16 promotes antitumor CD8(+) T cell exhaustion. Sci Immunol. 2022;7(71):eabh1873.

74. Lochner M, Berod L, Sparwasser T. Fatty acid metabolism in the regulation of T cell function. Trends Immunol. 2015;36(2):81-91.

75. Uche UU, Piccirillo AR, Kataoka S, Grebinoski SJ, D'Cruz LM, Kane LP. PIK3IP1/TrIP restricts activation of T cells through inhibition of PI3K/Akt. J Exp Med. 2018;215(12):3165-3179.

76. Kubo S, Kataria R, Yao Y, et al. Early B cell factor 4 modulates FAS-mediated apoptosis and promotes cytotoxic function in human immune cells. Proc Natl Acad Sci U S A. 2022;119(33):e2208522119.

List of figure captions

Figure 1. Human T cells can be transduced with equal efficacy regardless of pre-selection. (A) Primary T cells were isolated from PBMCs by selecting CD4+, CD8+, or both T cell types with MACS microbeads. Unselected T cells were included as a control. **(B)** T cells were transduced using replication incompetent retroviral vectors to secrete CD123xCD3. The CD123xCD3 molecule is composed of two scFvs (anti-CD123: 26292, anti-CD3: OKT3) connected by a GGGGSx3 linker. A transduction marker (CD20) was included. **(C)** Purity of selections was determined by flow cytometry on day 7 of culture. Differences between the proportions of CD4+ and CD8+ populations with and without transduction were assessed using the R package DirichletReg, **p ≤ 0.01. **(D)** Transduction was confirmed by flow cytometry using anti-CD20 antibodies. Statistical comparison was completed using two-way ANOVA (donor and selection) with Tukey tests for multiple comparisons. **(E)** CD123xCD3 expression and secretion was confirmed by ELISA on T-cell supernatant. Two-way ANOVA (donor and selection) with Tukey tests was used to compare selection groups. For **(C)**, **(D)**, and **(E)**, N = 3 or 4 independent transductions of unique T-cell donors. Non-transduced T cells were grown under the same conditions and for the same period of time as the respective ENG-T cells. No sel = no selection, NT = non-transduced, CD4/8 = CD4 and CD8-selected, ns = not significant.

Figure 2. T-cell short-term *in vitro* functionality is equivalent across selection groups. (A) CD4+ and CD8+ T-cell subsets (using CD4, CD8, CCR7, and CD45A as markers) were delineated on Day 7 after activation and plating. Differences in subset compositions were analysed using the R package DirichletReg. *p < 0.05, **p ≤ 0.01. A representative flow plot showing gating is provided. **(B)** Cytokine (IL-2 and IFNγ) present after 24-hour co-culture of T-cells with target cell lines (CD123-negative: K-562 and CD123+: K-562.CD123, MOLM-13, MV-4-11) was measured using ELISA. Statistical comparisons were completed using two-way ANOVA (donor and selection) with Tukey tests for multiple comparisons for selection groups co-cultured with each cell line. *p < 0.05. **(C)** Cytotoxicity was examined *in vitro* against target cell lines engineered to express firefly luciferase in 18-hour bioluminescence assays. Differences between selection groups at each E:T were assessed by three-way ANOVA (donor, selection, E:T) with Tukey tests for multiple comparisons using R. Asterisks indicate least significant p-value of experimental conditions vs. NT, *p < 0.05, **p ≤ 0.01, ***p ≤

0.001, ****p ≤ 0.0001. N = 3 independent transductions of unique T-cell donors. Non-transduced T cells were grown under the same conditions and for the same period of time as the respective ENG-T cells. No sel = no selection, NT = non-transduced, CD4/8 = CD4 and CD8-selected, ns = not significant, E:T = effector:target ratio.

Figure 3. CD4 and CD4/CD8 pre-selection of engineered T cells results in improved tumor control *in vivo*. (A) NSG mice were injected via tail vein with 5e4 firefly luciferase-expressing MOLM-13 cells. Seven days after AML injection, 5e6 ENG-T cells were injected also via tail vein. **(B)** AML burden was tracked in mice with weekly bioluminescence imaging and **(C)** quantified for each mouse. **(D)** Mouse survival was recorded. Log-rank Mantel-Cox tests were used to compare survival curves, *p < 0.05, **p ≤ 0.01. **(E)** The number of circulating T cells in peripheral blood (PB) was determined by flow cytometric analysis. For **(B)**, pink asterisks indicate from which animal blood was collected and processed for **(D)**. For **(C)** and **(E)**, dotted lines are individual animals and solid lines are the mean of each group. Non-transduced T-cell controls were unselected and grown under the same conditions as engineered cells. N = 4 per group. No sel = no selection, NT = non-transduced, CD4/8 = CD4 and CD8-selected.

Figure 4. CD4+ and CD8+ T cells are both required for durable anti-AML activity and T-cell survival. ENG-T cells and MOLM-13 marked with NLS-mCherry and NLS-GFP, respectively, were co-cultured in an Incucyte S3 live cell imaging system at an initial effector-to-target ratio of 1:1 per well. Cells were tracked in a 22-day serial stimulation assay (day 7 to 29 post-activation), with fresh target cells added every two days. **(A)** Cytotoxicity was determined by measurement of target cells per image, with viability calculated as a percentage of the total number of green objects recorded after re-stimulation. T cells per image quantified by detection of mCherry normalized to the number of red objects per image at time 0h (thick lines = means, vertical thin lines = standard error), 4 images per well, 3 wells per donor, 3 independent T-cell donors. **(B)** Comparative area under the curve (AUC) of T-cell expansions with indicated initial CD4:CD8 ENG-T cell ratios. 95% CI depicted for each condition. **(C)** Number of T cells per well at end experiment (D22) following 11 stimulations with target cells. CD4+ and CD8+ T-cell numbers measured using flow cytometry, *p < 0.05

representative of CD4+ cell number comparison across groups. **(D)** Cytotoxicity measured as in (A) 4 images per well, 3 wells per donor, comparing unselected products to those pre-selected of the most similar set CD4:8 ratios. **(E)** T-cell expansion per donor. No sel = no selection, CD4/8 = CD4 and CD8-selected. **(A-E)** N=3 unique T-cell donors.

Figure 5. Cytokine imprinting of non-selected ENG-T cells stunts survival during chronic stimulation. **(A)** T-cell subset composition (using CD4, CD8, CCR7, and CD45A as markers) was evaluated during manufacture (day 0 and 7) and after serial stimulation (day 17) by flow cytometry. The DirichletReg R package was used to determine group differences. **(B)** Exhaustion associated marker (PD-1, LAG-3, and TIM-3) expression was measured by flow cytometry before and after serial stimulation. Euler diagrams of average individual and overlapping marker expression were created using the eulerr R package. **(C)** Cytokines were detected and quantified in the supernatant of ENG-T cells during manufacture on day 1 (D1) and day 2 (D2) after activation and on day 17 (D17) after serial stimulation using a Luminex multiplex assay. A greater-than sign indicates at least one sample above the detection range. Statistical comparisons were done using two-way ANOVA (donor and selection) for each day. Samples with values above the detection range were not assessed statistically. *$p < 0.05$, **$p \leq 0.01$. For all plots, No sel = no selection, CD4/8 = CD4 and CD8-selection, N=3 independent T cell donors.

Figure 6. Transcriptional analysis highlights phenotypic differences in unselected vs. pre-selected ENG-T cell products. On day 7 of manufacture, 1e6 unselected or CD4/CD8-selected ENG-T cells tagged with NLS-mCherry were pelleted, RNA extracted, and bulk RNA sequenced. **(A)** Clustering of unselected and CD4/CD8-selected ENG-T derived from three unique T-cell donors was performed using the $\log_2$(FPKM+1) with expression normalized to Z-score. Two main clusters of genes were identified and further interrogated to identify genes of biological relevance. Expression level is coded from high (red) to low (green). **(B)** PCA analysis of unselected and CD4/CD8-selected ENG-T cells. **(C)** Signficant differences in gene expression between CD4/CD8 pre-selected vs. unselected ENG-T cells with upregulated (red) and downregulated (green)

genes annotated (adjusted p-value < 0.05, $|\log_2$ fold change$| > 1$). **(D)** Genes identified in differentially expressed clusters correlated to biological pathways identified with Enrichr.

Figure 7. Patient-derived CD4/CD8-selected ENG-T cells have decreased CD3-negative cell contamination. ENG-T cells were produced from banked peripheral blood samples from three patients treated at the Johns Hopkins Hospital. **(A)** T cells from patients 5800, 6034, and 6675 were activated on day 0 either without or after CD4/CD8-selection. CD3+, CD4+, CD8+, and disease populations were detected using flow cytometry. **(B)** Unselected and selected cells were transduced with an NLS-mCherry tagged ENG vector and expression of mCherry was detected on day 18 post-activation using flow cytometry. **(C)** CD3-negative cell and AML contamination was evaluated on day 18 post-activation using flow cytometry. **(D)** Expansion of unselected and selected products was evaluated by manual counting. **(E)** Production of CD123xCD3 was confirmed in the expansion media of transduced cell products by ELISA. **(F)** The presence of IL-1β, IL-6, and CXCL10 were detected in the T cell expansion media on the day following activation. Product from patient 6675 was not evaluated due to high disease contamination. No sel = no selection, CD4/8 = CD4 and CD8-selected.

Figure 1

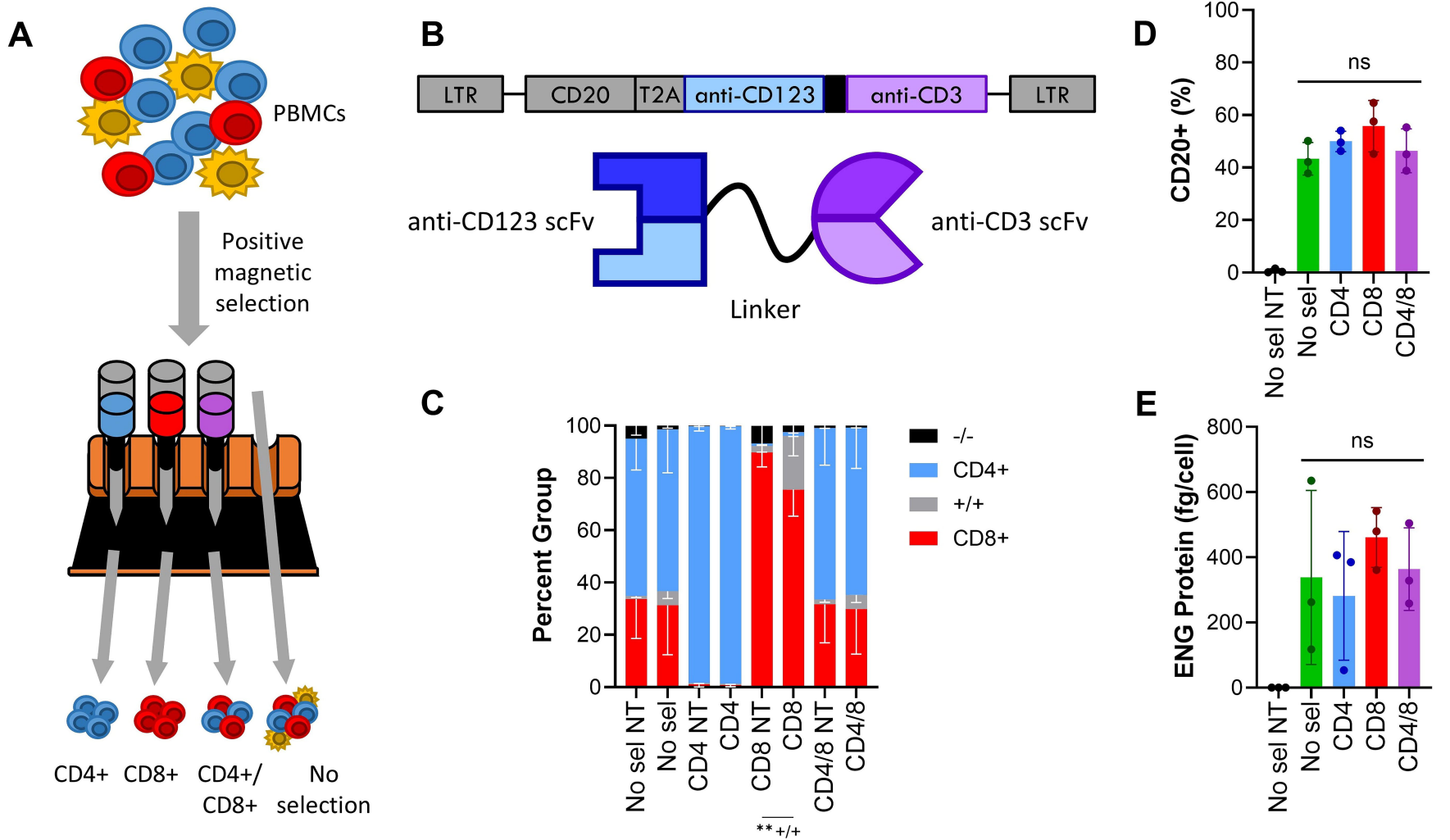
A
PBMCs
Positive magnetic selection
CD4+
CD8+
CD4+/ CD8+
No selection
B
LTR
CD20
T2A
anti-CD123
anti-CD3
LTR
anti-CD123 scFv
anti-CD3 scFv
Linker
C
Percent Group
-/-
CD4+
+/+
CD8+
No sel NT
No sel
CD4 NT
CD4
CD8 NT
CD8
CD4/8 NT
CD4/8
**+/+
D
CD20+ (%)
ns
No sel NT
No sel
CD4
CD8
CD4/8
E
ENG Protein (fg/cell)
ns
No sel NT
No sel
CD4
CD8
CD4/8

Figure 2

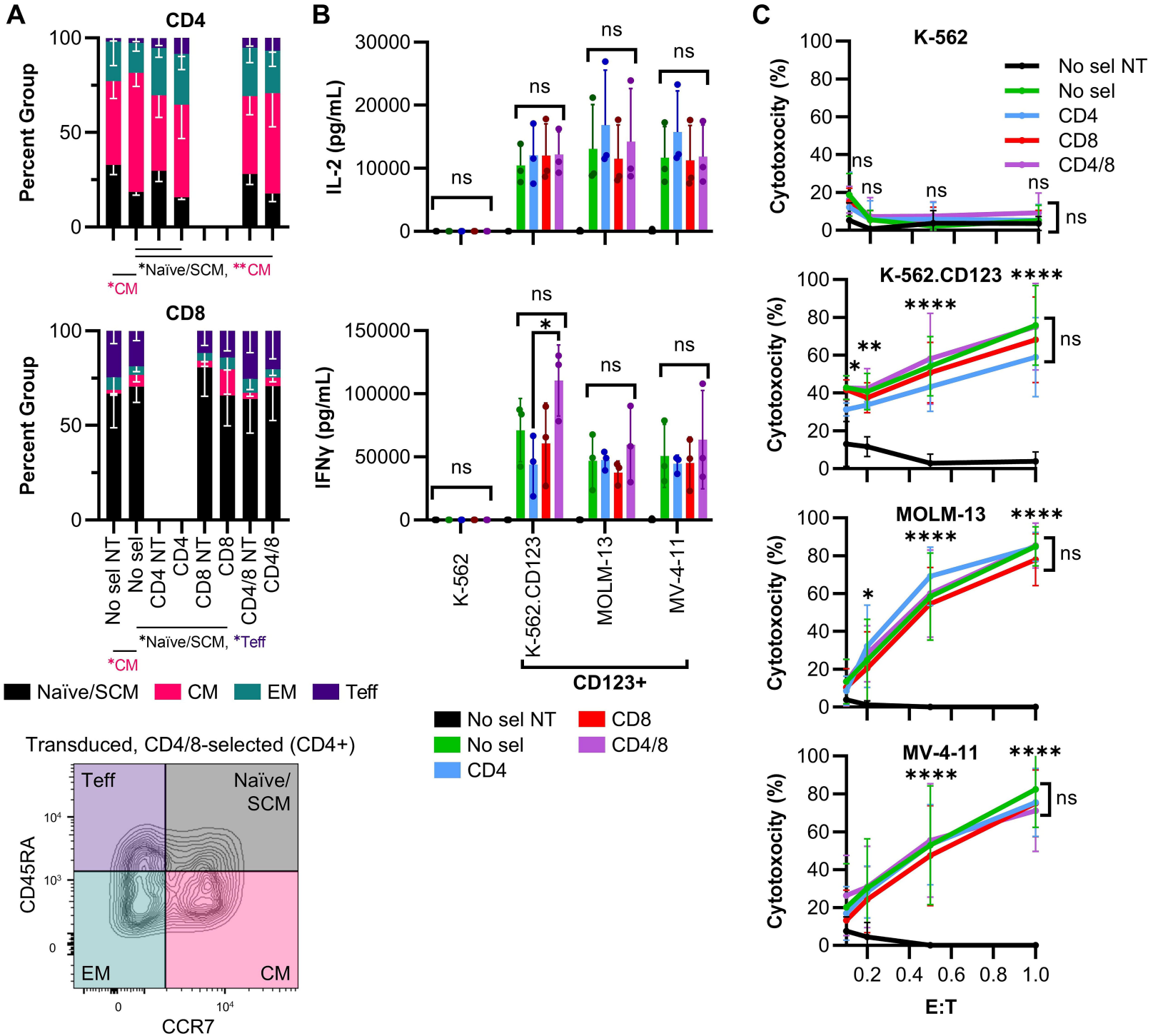
A
CD4
Percent Group
100
50
0
*Naïve/SCM, **CM
*CM
CD8
Percent Group
100
50
0
No sel NT
No sel
CD4 NT
CD4
CD8 NT
CD8
CD4/8 NT
CD4/8
*Naïve/SCM, *Teff
*CM
Naïve/SCM
CM
EM
Teff
Transduced, CD4/8-selected (CD4+)
Teff
Naïve/
SCM
EM
CM
CD45RA
CCR7
10⁴
10³
0
0
10⁴
B
IL-2 (pg/mL)
30000
20000
10000
0
ns
IFNγ (pg/mL)
150000
100000
50000
0
*
K-562
K-562.CD123
MOLM-13
MV-4-11
CD123+
No sel NT
No sel
CD4
CD8
CD4/8
C
K-562
Cytotoxicity (%)
No sel NT
No sel
CD4
CD8
CD4/8
K-562.CD123 ****
MOLM-13 ****
MV-4-11 ****
E:T
0.2
0.4
0.6
0.8
1.0

Figure 3

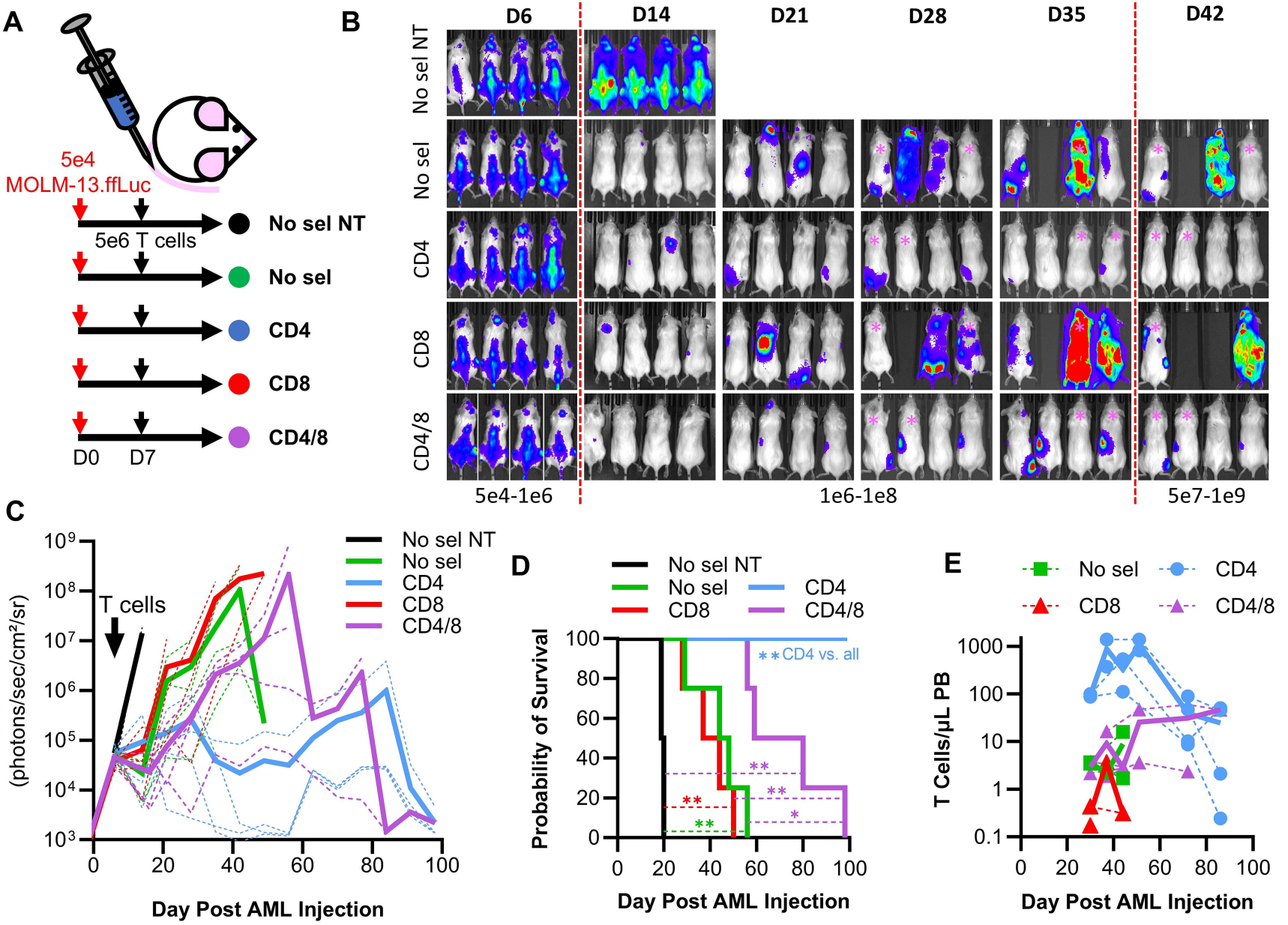
A
5e4
MOLM-13.ffLuc
5e6 T cells
No sel NT
No sel
CD4
CD8
CD4/8
D0
D7
B
D6
D14
D21
D28
D35
D42
No sel NT
No sel
CD4
CD8
CD4/8
5e4-1e6
1e6-1e8
5e7-1e9
C
Radiance
(photons/sec/cm²/sr)
T cells
No sel NT
No sel
CD4
CD8
CD4/8
Day Post AML Injection
D
Probability of Survival
No sel NT
No sel
CD8
CD4
CD4/8
**CD4 vs. all
Day Post AML Injection
E
No sel
CD4
CD8
CD4/8
T Cells/µL PB
Day Post AML Injection

Figure 4

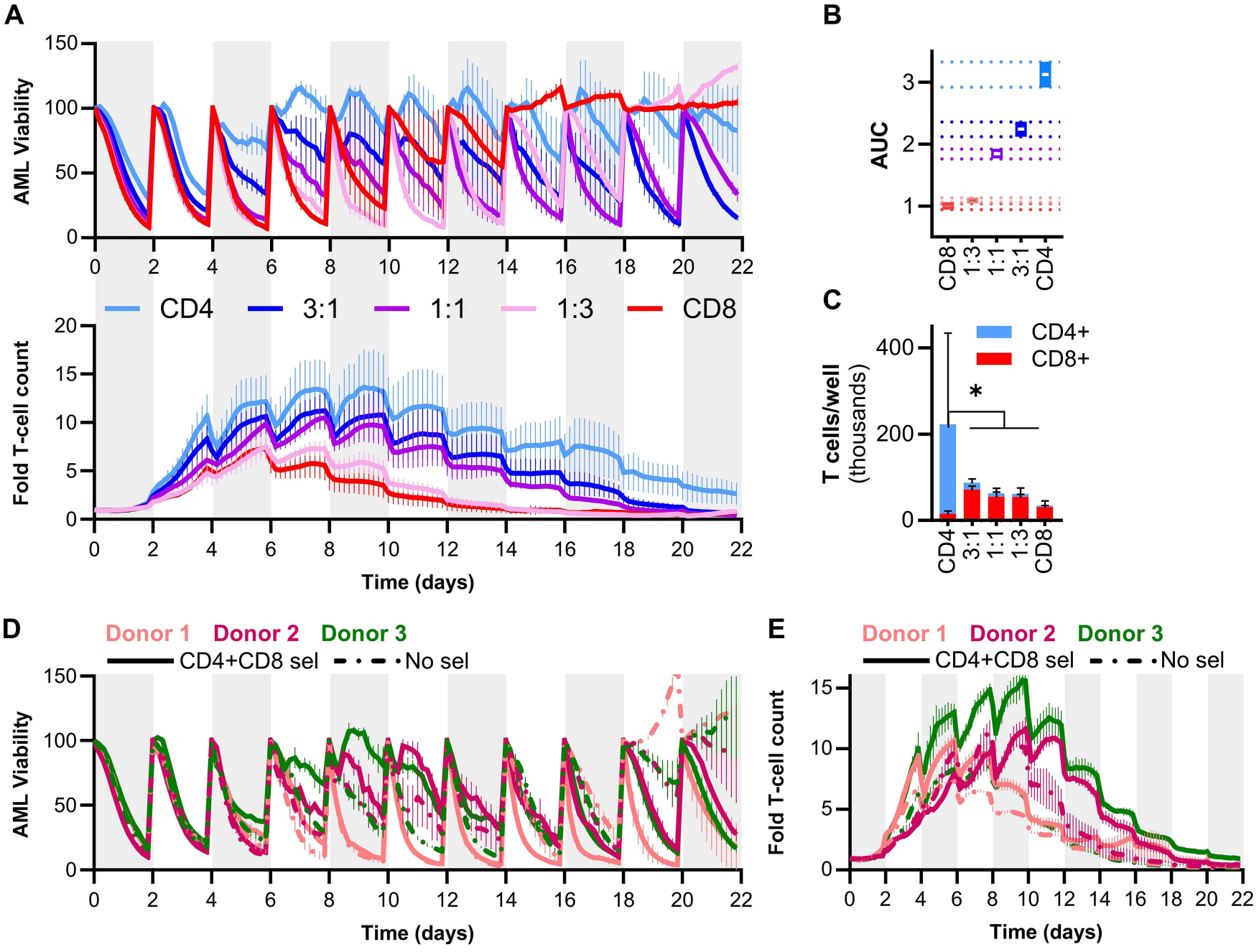
A
AML Viability
150
100
50
0
0 2 4 6 8 10 12 14 16 18 20 22
CD4
3:1
1:1
1:3
CD8
Fold T-cell count
20
15
10
5
0
Time (days)
B
AUC
3
2
1
CD8
1:3
1:1
3:1
CD4
C
T cells/well
(thousands)
400
200
0
CD4+
CD8+
*
CD4
3:1
1:1
1:3
CD8
D
Donor 1
Donor 2
Donor 3
CD4+CD8 sel
No sel
AML Viability
Time (days)
E
Donor 1
Donor 2
Donor 3
CD4+CD8 sel
No sel
Fold T-cell count
Time (days)

Figure 5

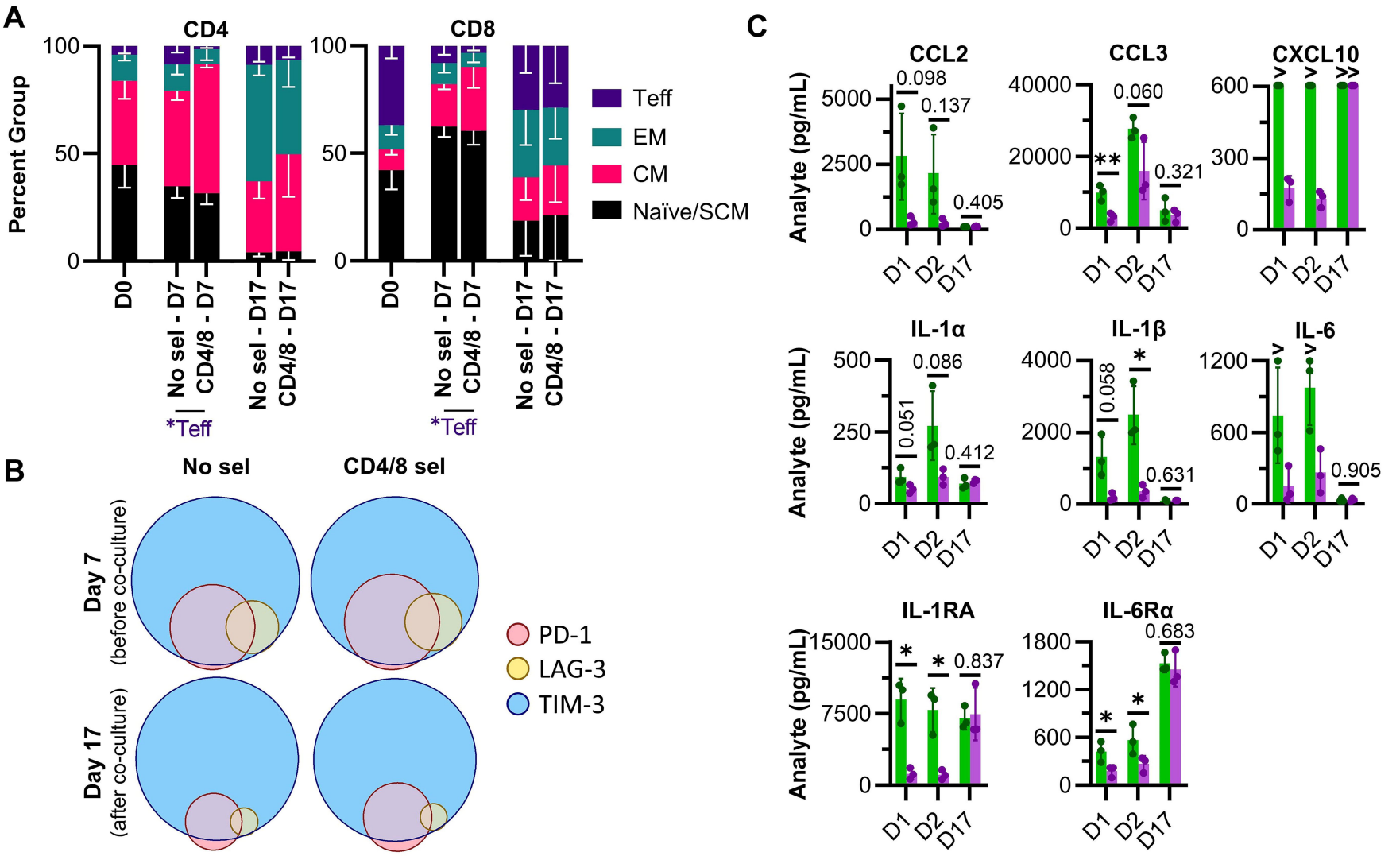
A
CD4
CD8
Percent Group
100
50
0
Teff
EM
CM
Naïve/SCM
D0
No sel - D7
CD4/8 - D7
No sel - D17
CD4/8 - D17
*Teff
B
No sel
CD4/8 sel
Day 7
(before co-culture)
Day 17
(after co-culture)
PD-1
LAG-3
TIM-3
C
CCL2
CCL3
CXCL10
IL-1α
IL-1β
IL-6
IL-1RA
IL-6Rα
Analyte (pg/mL)
D1
D2
D17
0.098
0.137
0.405
0.060
0.321
**
0.086
0.051
0.412
0.058
0.631
0.905
0.837
0.683

Figure 6

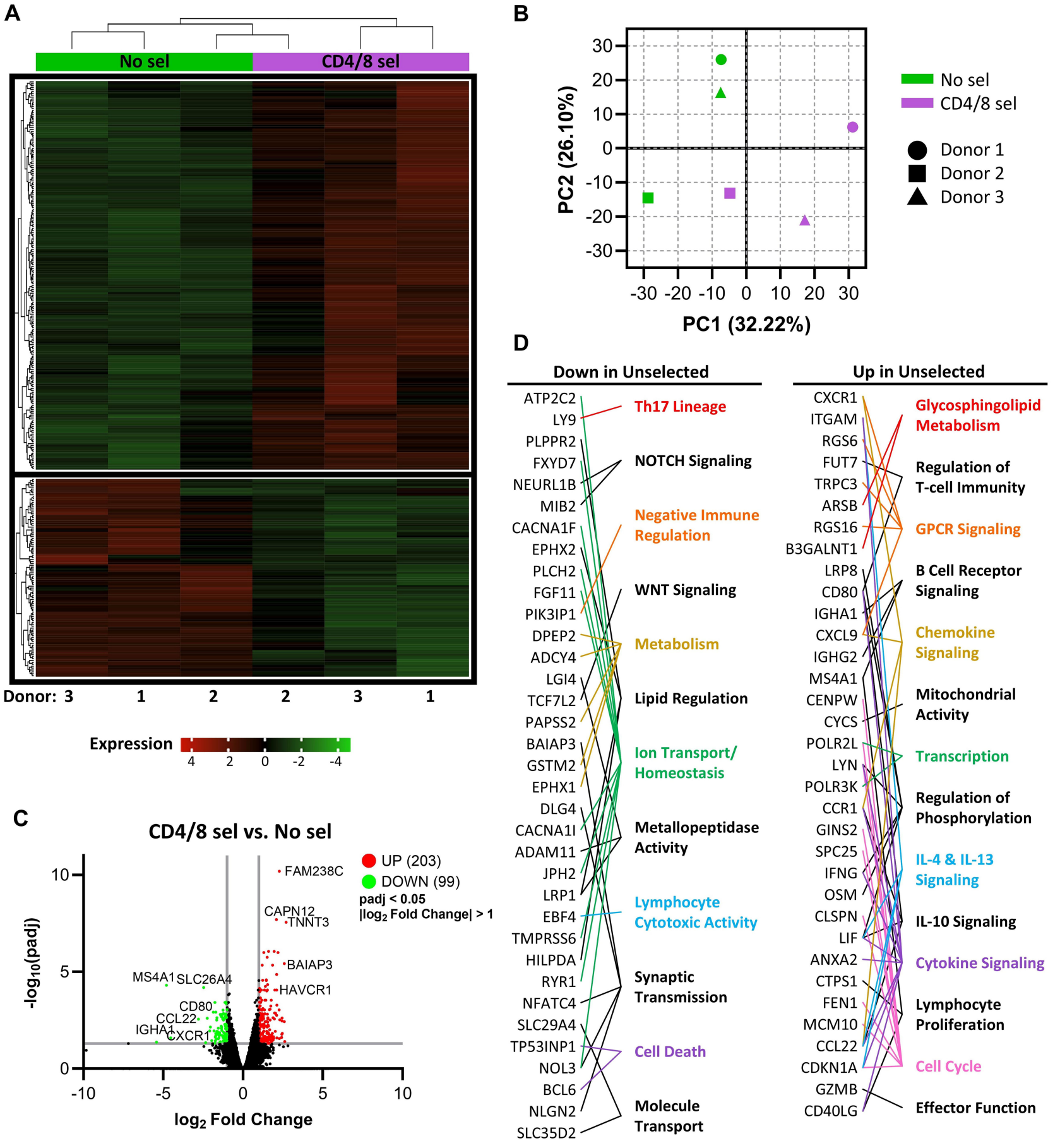
A
No sel
CD4/8 sel
Donor: 3 1 2 2 3 1
Expression
4 2 0 -2 -4
B
PC2 (26.10%)
PC1 (32.22%)
No sel
CD4/8 sel
Donor 1
Donor 2
Donor 3
C
CD4/8 sel vs. No sel
UP (203)
DOWN (99)
padj < 0.05
|log2 Fold Change| > 1
-log10(padj)
log2 Fold Change
FAM238C
CAPN12
TNNT3
BAIAP3
HAVCR1
MS4A1
SLC26A4
CD80
CCL22
IGHA1
CXCR1
D
Down in Unselected
Up in Unselected
ATP2C2
LY9
PLPPR2
FXYD7
NEURL1B
MIB2
CACNA1F
EPHX2
PLCH2
FGF11
PIK3IP1
DPEP2
ADCY4
LGI4
TCF7L2
PAPSS2
BAIAP3
GSTM2
EPHX1
DLG4
CACNA1I
ADAM11
JPH2
LRP1
EBF4
TMPRSS6
HILPDA
RYR1
NFATC4
SLC29A4
TP53INP1
NOL3
BCL6
NLGN2
SLC35D2
Th17 Lineage
NOTCH Signaling
Negative Immune Regulation
WNT Signaling
Metabolism
Lipid Regulation
Ion Transport/ Homeostasis
Metallopeptidase Activity
Lymphocyte Cytotoxic Activity
Synaptic Transmission
Cell Death
Molecule Transport
CXCR1
ITGAM
RGS6
FUT7
TRPC3
ARSB
RGS16
B3GALNT1
LRP8
CD80
IGHA1
CXCL9
IGHG2
MS4A1
CENPW
CYCS
POLR2L
LYN
POLR3K
CCR1
GINS2
SPC25
IFNG
OSM
CLSPN
LIF
ANXA2
CTPS1
FEN1
MCM10
CCL22
CDKN1A
GZMB
CD40LG
Glycosphingolipid Metabolism
Regulation of T-cell Immunity
GPCR Signaling
B Cell Receptor Signaling
Chemokine Signaling
Mitochondrial Activity
Transcription
Regulation of Phosphorylation
IL-4 & IL-13 Signaling
IL-10 Signaling
Cytokine Signaling
Lymphocyte Proliferation
Cell Cycle
Effector Function

Figure 7

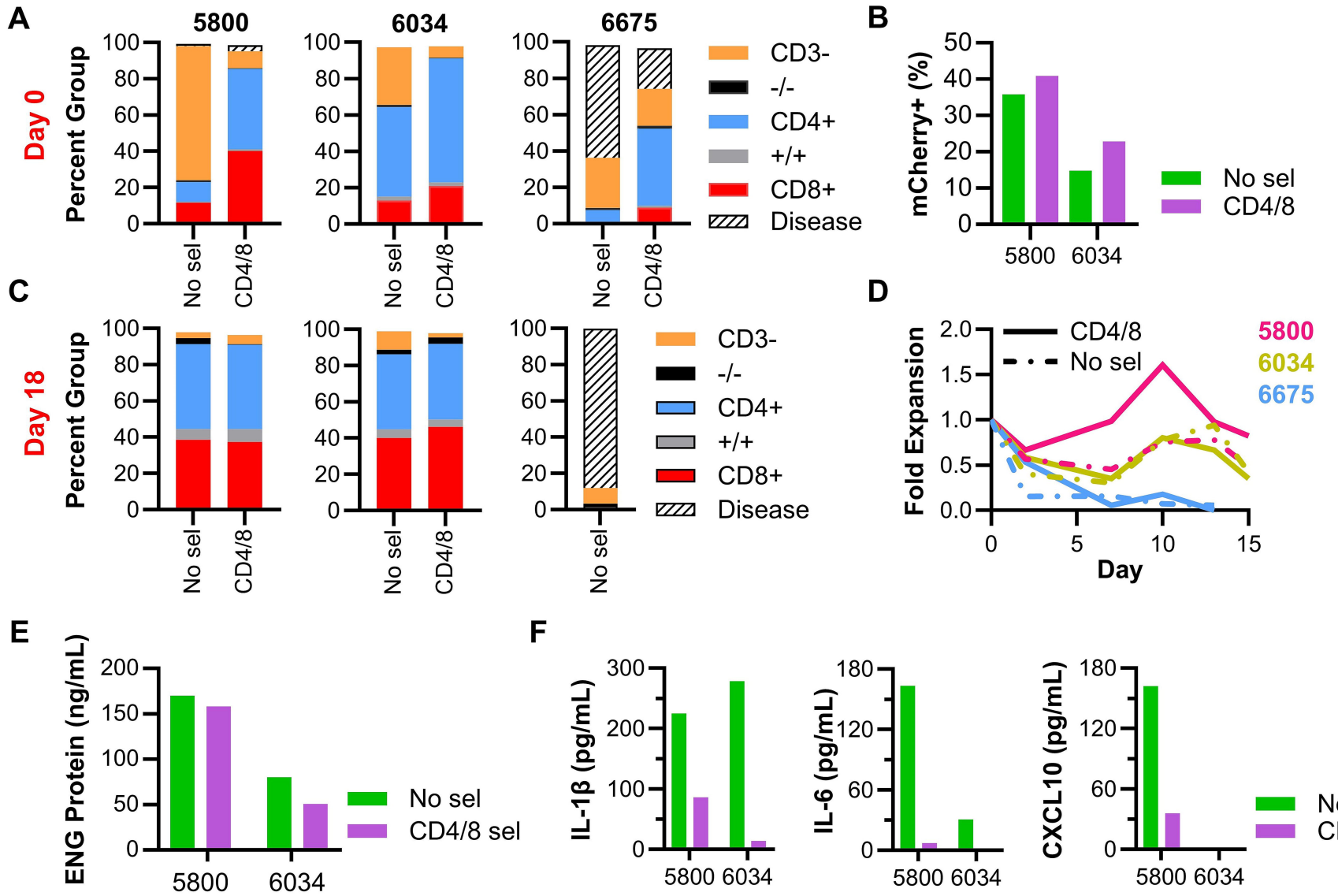
A
5800
6034
6675
Day 0
Percent Group
100
80
60
40
20
0
No sel
CD4/8
CD3-
-/-
CD4+
+/+
CD8+
Disease
B
mCherry+ (%)
50
40
30
20
10
0
5800
6034
No sel
CD4/8
C
Day 18
Percent Group
D
Fold Expansion
2.0
1.5
1.0
0.5
0.0
CD4/8
No sel
5800
6034
6675
0
5
10
15
Day
E
ENG Protein (ng/mL)
200
150
100
50
0
5800
6034
No sel
CD4/8 sel
F
IL-1β (pg/mL)
300
200
100
0
IL-6 (pg/mL)
180
120
60
0
CXCL10 (pg/mL)
5800 6034
No sel
CD4/8

Supplemental methods

Flow cytometry

FACSCelesta (BD Biosciences) and Attune NxT (ThermoFisher) flow cytometers were used with data analyzed in FlowJo (v10.8.1). All samples were washed with FACS buffer or PBS when using live/dead stains.

Antibodies used are listed in **Table S2**.

Cell line culture

All cell lines were maintained in a humidified incubator at 37°C with 5% CO_2. MV-4-11 and K-562 were obtained from the American Type Culture Collection (ATCC) and maintained in Iscove's Modified Dulbecco's Medium (IMDM, Gibco) supplemented with 10% fetal bovine serum (FBS, Hyclone Laboratories). MOLM-13 was maintained in Roswell Park Memorial Institute (RPMI, Gibco) complete with 10% FBS and was originally purchased from the German Collection of Microorganisms and Cell Cultures (DSMZ). Cell lines were transduced with retroviral vectors containing various reporters encoded in pSFG plasmids to enable tracking in experiments. All transduced cell lines were sorted using a BD FACSMelody Cell Sorter and confirmed positive for reporters by flow or by using substrates for enzymes when applicable. HEK293T cells used for viral production were maintained in Dulbecco's Modified Eagle Medium (DMEM, Gibco) complete with 10% FBS and were originally obtained from ATCC. Cell lines were authenticated (Johns Hopkins Genetic Resources Core Facility) and test ed for mycoplasma (MycoAlert Detection kit, Lonza) when new cell lines were established after transduction and when stock vials were frozen down.

CD123xCD3 transgene generation

The CD123xCD3 sequence was subcloned into a pMSGV backbone. A sequence encoding a stable marker (full length CD20) was followed by a viral skip sequence (T2A) and a CD123-specific single chain fragment variable (scFv, 26292)[1] conjugated to a CD3-specific scFv derived from the OKT3 clone (Thermo Fisher Scientific) with a serine-glycine linker (GGGGSx3). In-Fusion cloning (Takara Bio) was used to generate a plasmid tagged with nuclear localized mCherry in place of CD20.

Plasmids were amplified in Stellar chemically competent *Escherichia coli* (Takara Bio) and isolated using DNA mini or midi kits (QIAGEN) following the manufacturer's instructions. Sequence fidelity was verified by Sanger sequencing (Johns Hopkins Genetic Resources Core Facility).

Viral production

Research-grade retroviral vector was produced to align with GMP guidelines by the Biopharmaceutical Development Program (Frederick National Laboratory for Cancer Research, Leidos Biomedical Research, Inc).

All vector used was from Lot RD20220810. For CD123xCD3 vectors tagged with nuclear localized mCherry (ENG.NLSmCh) and reporter vectors used to transduce cell lines, replication incompetent RD114 -pseudotyped retroviral vectors were produced in-house using HEK293T cells. Cells were transfected with GeneJuice Transfection Reagent (Sigma-Aldrich) and 10µg of total DNA (3:3:2 of packaging genes, RD114 envelope, and plasmid encoding bispecific). Supernatant containing virus was harvested after 48h, passed through 0.45µm syringe filters, and snap frozen before storing at -80°C.

ENG-T cell production

Peripheral blood mononuclear cells (PBMCs) were isolated from fresh healthy donor blood by layering over Lymphoprep (STEMCELL Technologies) and centrifuging. Buffy coat was collected and washed. PBMCs were frozen in complete RPMI with 10% DMSO and stored long-term in liquid nitrogen. CD4+ and CD8+ cells were isolated from thawed PBMCs using CD4 or CD8 MACS microbeads (Miltenyi Biotec). Briefly, PBMCs were passed through a pre-separation cell strainer (30µm) and incubated with anti-CD4, anti-CD8, or a 1:1 mixture of both microbeads in MACS buffer. Cell suspensions were filtered through lymphocyte selection columns placed in a MACS magnet. Bound cells were washed and then eluted. After purity was confirmed with flow cytometry, selected cells (CD4, CD8, CD4/CD8) and unselected cells were plated on anti-CD3 and anti-CD28 antibody-coated 24-well plates in RPMI complete with 10% FBS and 2mM of GlutaMAX (Gibco). The day following activation, cells were fed with fresh complete medium supplemented with 10ng/mL

recombinant human IL-7 (rhIL-7) and 5ng/mL recombinant human IL-15 (rhIL-15, Biological Resources Branch Preclinical Biorepository, National Cancer Institute). Two days following activation, cells were transduced by plating on virus immobilized to 24-well plates coated with RetroNectin (Takara Bio). Cells were removed from RetroNectin on day 4 after activation and expanded in 24-well tissue culture-treated plates. T cells were split every 2-3 days and refreshed with complete RPMI supplemented with rhIL-7 and rhIL-15.

Transduction efficiency

Transduction efficiency of ENG-T cells was determined by staining for surface CD20. Transduction efficiency of ENG.NLSmCh-T cells was measured by mCherry detection via FACS. Expression was evaluated on day 7 for healthy donor and on day 6 or day 18 for patient-derived ENG-T cells.

Cytotoxicity

CD123+ and CD123-negative target cell lines engineered to express firefly luciferase (ffLuc) were plated with effector cells in a 96-well plate. Cells were incubated for 18h before adding D-luciferin (Thermo Fisher Scientific, 150µg/mL). Bioluminescence was measured with a BMG CLARIOstar Plus microplate reader. Cytotoxicity was calculated as the reduction in bioluminescence compared to target-only wells using Microsoft Excel Version 16.94. Patient-derived ENG-T cells were co-cultured 1:1 with autologous AML for 72h. Remaining CD33+ cells were enumerated using fluorophore-conjugated antibodies after staining with a green live/dead stain.

Human AML xenograft mouse model

Female NOD.Cg-Prkdc^{scid}Il2rg^{tm1Wjl}/SzJ (NSG) mice 8-10 weeks old were obtained from an internal colony originally established from the Jackson Laboratory. All protocols were approved by the Johns Hopkins Institutional Animal Care and Use Committee. Mice were injected i.v. with 5e4 MOLM-13.ffLuc cells on day 0 and were treated i.v. on day 7 with unmodified T cells or ENG-T cells produced from healthy whole PBMC, CD4+, CD8+, or CD4+/CD8+ starting material. Before treatment, tumor burden was assessed by bioluminescence imaging and mice were cohorted to eliminate variability. Tumor burden was detected by weekly imaging using an Xenogen IVIS Spectrum. Radiance was quantified

using Living Image v4.7.3. Blood was collected from half of the mice each week via submandibular puncture in EDTA-tubes (RAM Scientific). Mice were monitored clinically for 100 days and sacrificed at humane endpoints.

ENG-T cell production from AML patient biospecimens

ENG.NLSmCh-T cells were produced from biospecimens harvested and banked from five adult patients previously treated at the Johns Hopkins Hospital and consented to the institutional IRB-approved biobanking protocol, J0969. Three of the biospecimens used for *ex vivo* manufacture were PBMCs (patient numbers: 5800, 6034, and 6675) and two were bone marrow mononuclear cells (BMMCs, patient numbers: 4293 and 4316). All patients had disease with a clinical phenotype consistent with AML (**Table S8**). Cells were either unselected or selected for CD4+ and CD8+ cells prior to activation. All PBMC samples were from the day of diagnosis of AML. T cells from patient 4293 were expanded from post-treatment BMMCs while T cells from patient 4316 were expanded from BMMCs isolated from the diagnostic bone marrow sample. Matched autologous AML used in preclinical cytotoxicity assays was obtained from diagnostic bone marrow aspirates. Fold expansion of cells produced from patient samples was determined by manual counting.

Murine peripheral blood (PB) processing

After collection, the volume of PB was recorded. Red cells were lysed with RBC lysis buffer (eBioscience). All samples were blocked with mouse Fc block (BD Biosciences) before antibody staining. Samples were washed and resuspended in the same volume. Samples were run at a set speed and time to acquire a known volume. The acquired volume of sample was used to calculate the volume of blood assayed per mouse.

RNA sequencing

On day 7 after activation, 1e6 unselected or CD4/CD8 pre-selected healthy donor ENG.NLSmCh-T cells were collected. Total RNA was isolated using a RNeasy mini kit (QIAGEN) following the

manufacturer's protocol. RNAseq was performed by Novogene using a non-directional library and a sequencing depth of 20M reads. Enrichment of biologically relevant pathways were identified using Enrichr.[2,3]

1. Du X, Ho M, Pastan I. New immunotoxins targeting CD123, a stem cell antigen on acute myeloid leukemia cells. *J Immunother*. 2007;30(6):607-613.

2. Chen EY, Tan CM, Kou Y, et al. Enrichr: interactive and collaborative HTML5 gene list enrichment analysis tool. *BMC Bioinformatics*. 2013;14:128.

3. Kuleshov MV, Jones MR, Rouillard AD, et al. Enrichr: a comprehensive gene set enrichment analysis web server 2016 update. *Nucleic Acids Res*. 2016;44(W1):W90-97.

Table S1. FDA-approved engineered T-cell therapies

Product	AKA	Construct	Initial Approval	Manufacturer	Activation	Transduction	Selection	Ref
tisagenlecleucel	tisa-cel, KYMRIAH	αCD19. 41BB.ζ	2017	Novartis	anti-CD3/CD28 antibody-coated microbeads	lentivirus	No	[20]
axicabtagene ciloleucel	axi-cel, YESCARTA	αCD19. CD28.ζ	2017	Kite Pharma	anti-CD3 antibody and IL-2	retrovirus	No	[21]
brexucabtagene autoleucel	brexu-cel, TECARTUS	αCD19. CD28.ζ	2020	Kite Pharma	anti-CD3 and anti-CD28 antibodies and IL-2	retrovirus	Positive selection of CD4+ and CD8+	[13,22]
idecabtagene vicleucel	ide-cel, ABECMA	αBCMA. 41BB.ζ	2021	Celgene	anti-CD3 and anti-CD28 antibodies and IL-2	lentivirus	No	[23,24]
lisocabtagene maraleucel	liso-cel, BREYANZI	αCD19. 41BB.ζ	2021	Celgene and Juno Therapeutics	anti-CD3/CD28 antibody-coated microbeads	lentivirus	Positive selection of CD4+ and CD8+, separately	[25,26]
ciltacabtagene autoleucel	cilta-cel, CARVYKTI	αBCMA. 41BB.ζ	2022	Janssen Biotech	CD3/CD28-stimulating microbeads and IL-2	lentivirus	Negative selection of pan T cells	[27,28]
afamitresgene autoleucel	afami-cel, TECELRA	αMAGE-A4 TCR	2024	Adaptimmune	CD3/CD28-stimulating microbeads	lentivirus	No	[29,30]

Table S2. Antibody list

Antibody	Fluorophore	Reference
T-cell activation		
CD3		Miltenyi: 130-093-387
CD28		BD: 555725
ELISA		
Goat Anti-Mouse IgG, $F(ab')_2$ fragment specific		Jackson Immunoresearch: 115-006-072
Bovine anti-goat HRP		Jackson Immunoresearch 805-035-180
Purity panel – healthy donor day 0 and all patient-derived cells		
CD3	PerCP-Vio700	Miltenyi: 130-113-132
CD4	APC-Vio770	Miltenyi: 130-113-251
CD8	PE	Miltenyi: 130-113-158
CD33	VioBlue	Miltenyi: 130-111-141
CD123	BB515	BD: 567715
CD20	BV786	BD: 743611
Purity panel – healthy donor day 7		
CD4	PerCP-Cy5.5	BD: 566923
CD8	FITC	BD: 347313
CD33	BV421	BD: 744761
CD123	BV786	BD: 564196
CD20	APC	BD: 559776
Immunophenotype panel		
CD4	BV750	BD: 747176
CD8	BV421	BD: 562428
CCR7	APC	BD: 566762
CD45RA	PE	BD: 555489
LIVE/DEAD		ThermoFisher: L34969
Immunophenotype panel with transduction marker		
CD4	PerCP-Cy5.5	BD: 560650
CD8	BV421	BD: 562428
CCR7	APC	BD: 566762
CD45RA	BV510	BD: 563031
CD20	PE	BD: 555623
Exhaustion panel		
PD-1	Alexa 647	BD: 560838
LAG-3	PE	BD: 565616
TIM-3	BV421	BD: 565562
CD4	BV750	BD: 747176
CD8	APC-Cy7	BD: 557760
LIVE/DEAD		ThermoFisher: L34969
Murine peripheral blood panel		
hCD45	FITC	BD: 555482
hCD20	APC	BD: 559776
hCD33	BV421	BD: 744761

Table S3. Parameters for AML viability curves fit to each stimulation of pre-selected, set ratio ENG-T cells

	CD4	3:1	1:1	1:3	CD8
Stimulation 1					
Best-fit B0	105.5	105.4	105.3	104.5	104
(95% CI)	(103.9 to 107.0)	(103.6 to 107.2)	(102.9 to 107.7)	(101.8 to 107.2)	(99.62 to 108.3)
Best-fit B1	-32.64	-53.7	-72.54	-83.5	-90.07
(95% CI)	(-36.60 to -28.68)	(-58.31 to -49.09)	(-78.63 to -66.45)	(-90.35 to -76.65)	(-101.1 to -79.08)
Best-fit B2	-5.807	1.737	10.73	16.41	19.88
(95% CI)	(-7.888 to -3.726)	(-0.6863 to 4.161)	(7.526 to 13.93)	(12.82 to 20.01)	(14.11 to 25.65)
R^2	0.9843	0.9843	0.9755	0.9702	0.9521
Stimulation 2					
Best-fit B0	179.5	331.4	394.5	420.4	415.8
(95% CI)	(137.5 to 221.5)	(296.5 to 366.2)	(361.0 to 428.0)	(387.3 to 453.5)	(361.8 to 469.8)
Best-fit B1	-31.11	-142.5	-190.4	-211.1	-206.8
(95% CI)	(-60.69 to -1.535)	(-167.0 to -117.9)	(-213.9 to -166.8)	(-234.3 to -187.8)	(-244.8 to -168.8)
Best-fit B2	-2.304	15.79	23.63	27.16	26.24
(95% CI)	(-7.355 to 2.747)	(11.60 to 19.98)	(19.60 to 27.65)	(23.19 to 31.14)	(19.75 to 32.74)
R^2	0.9183	0.9552	0.9628	0.9643	0.9417
Stimulation 3					
Best-fit B0	397.4	704	1117	1252	1173
(95% CI)	(207.6 to 587.2)	(580.6 to 827.5)	(1055 to 1178)	(1170 to 1334)	(1015 to 1330)
Best-fit B1	-118.8	-233.7	-396.6	-454.8	-420.4
(95% CI)	(-196.8 to -40.86)	(-284.4 to -183.0)	(-421.8 to -371.5)	(-488.5 to -421.2)	(-484.9 to -355.8)
Best-fit B2	10.84	20.46	35.67	41.56	37.96
(95% CI)	(2.926 to 18.76)	(15.31 to 25.61)	(33.12 to 38.23)	(38.15 to 44.98)	(31.41 to 44.52)
R^2	0.2922	0.8639	0.9818	0.9696	0.9306
Stimulation 4					
Best-fit B0	-678.5	233.3	921.7	1562	2081
(95% CI)	(-1080 to -277.2)	(-467.6 to 934.1)	(567.9 to 1275)	(1148 to 1977)	(1771 to 2391)
Best-fit B1	225.7	-24.89	-218.7	-402.8	-547
(95% CI)	(109.1 to 342.3)	(-228.5 to 178.8)	(-321.5 to -115.9)	(-523.2 to -282.5)	(-637.1 to -456.9)
Best-fit B2	-16.16	0.3576	13.47	26.32	36.15
(95% CI)	(-24.58 to -7.734)	(-14.35 to 15.07)	(6.046 to 20.90)	(17.63 to 35.01)	(29.64 to 42.65)
R^2	0.1288	0.2097	0.7412	0.7628	0.9303
Stimulation 5					
Best-fit B0	-1907	118.2	964.8	3600	2955
(95% CI)	(-2509 to -1304)	(-1718 to 1955)	(-371.9 to 2302)	(3044 to 4156)	(1783 to 4127)
Best-fit B1	456.9	4.119	-176.4	-763.8	-612
(95% CI)	(321.3 to 592.4)	(-409.0 to 417.2)	(-477.1 to 124.3)	(-889.0 to -638.7)	(-875.7 to -348.3)
Best-fit B2	-25.9	-1.027	8.343	40.62	31.87
(95% CI)	(-33.50 to -18.31)	(-24.18 to 22.13)	(-8.513 to 25.20)	(33.61 to 47.63)	(17.09 to 46.65)
R^2	0.3332	0.05155	0.2843	0.8535	0.688
Stimulation 6					
Best-fit B0	-2707	214.3	2309	5371	2012
(95% CI)	(-4512 to -902.4)	(-2588 to 3017)	(447.9 to 4171)	(4648 to 6095)	(-966.3 to 4991)
Best-fit B1	527.4	-2.451	-378.1	-937.3	-319.8
(95% CI)	(196.1 to 858.8)	(-516.9 to 512.0)	(-719.8 to -36.44)	(-1070 to -804.4)	(-866.5 to 227.0)
Best-fit B2	-24.73	-0.997	15.66	40.95	12.9
(95% CI)	(-39.90 to -9.554)	(-24.55 to 22.56)	(0.009233 to 31.30)	(34.86 to 47.03)	(-12.14 to 37.93)
R^2	0.1637	0.1325	0.4494	0.9	0.3476
Stimulation 7					
Best-fit B0	-3934	1958	6047	5691	163.2
(95% CI)	(-7574 to -293.7)	(-2424 to 6339)	(4398 to 7697)	(5075 to 6306)	(-2322 to 2648)
Best-fit B1	641.8	-266.8	-894	-827.8	20.28
(95% CI)	(77.37 to 1206)	(-946.2 to 412.5)	(-1150 to -638.2)	(-923.3 to -732.3)	(-365.1 to 405.6)

Best-fit B2 (95% CI)	-25.47 (-47.31 to -3.625)	9.297 (-17.00 to 35.59)	33.14 (23.24 to 43.03)	30.17 (26.47 to 33.87)	-2.113 (-17.03 to 12.80)
R^2	0.1151	0.133	0.7175	0.9646	0.541
Stimulation 8					
Best-fit B0 (95% CI)	-3337 (-7831 to 1157)	3899 (-664.1 to 8462)	7093 (5476 to 8710)	-421.7 (-1699 to 855.5)	1533 (484.9 to 2582)
Best-fit B1 (95% CI)	486.5 (-116.7 to 1090)	-481.1 (-1094 to 131.3)	-905 (-1122 to -687.9)	109.6 (-61.83 to 281.0)	-202.4 (-343.1 to -61.67)
Best-fit B2 (95% CI)	-17.2 (-37.42 to 3.014)	14.96 (-5.563 to 35.49)	28.94 (21.66 to 36.21)	-5.155 (-10.90 to 0.5905)	7.139 (2.422 to 11.86)
R^2	0.2183	0.3021	0.8422	0.8955	0.5559
Stimulation 9					
Best-fit B0 (95% CI)	-5197 (-12831 to 2437)	4672 (-2111 to 11455)	10149 (8202 to 12096)	1247 (-136.8 to 2630)	-1141 (-2127 to -154.3)
Best-fit B1 (95% CI)	647.3 (-255.9 to 1551)	-516.7 (-1319 to 285.9)	-1154 (-1384 to -923.2)	-97.49 (-261.2 to 66.20)	140.7 (23.95 to 257.4)
Best-fit B2 (95% CI)	-19.76 (-46.46 to 6.930)	14.38 (-9.335 to 38.10)	32.82 (26.01 to 39.63)	1.63 (-3.207 to 6.468)	-3.947 (-7.396 to -0.4982)
R^2	0.1015	0.1968	0.8699	0.9171	0.5053
Stimulation 10					
Best-fit B0 (95% CI)	-5344 (-13664 to 2976)	9925 (6689 to 13161)	4655 (1389 to 7921)	2599 (85.37 to 5112)	772.4 (417.7 to 1127)
Best-fit B1 (95% CI)	587.9 (-292.4 to 1468)	-1001 (-1343 to -658.3)	-439.3 (-784.8 to -93.81)	-271.6 (-537.5 to -5.675)	-72.46 (-110.0 to -34.93)
Best-fit B2 (95% CI)	-15.86 (-39.13 to 7.401)	25.25 (16.21 to 34.30)	10.35 (1.222 to 19.48)	7.379 (0.3506 to 14.41)	1.95 (0.9577 to 2.941)
R^2	0.05457	0.7956	0.7991	0.1726	0.3763
Stimulation 11					
Best-fit B0 (95% CI)	-1265 (-14261 to 11730)	9627 (6506 to 12747)	523.6 (-2148 to 3195)	-2139 (-3544 to -734.0)	58.15 (-1855 to 1972)
Best-fit B1 (95% CI)	140.5 (-1103 to 1384)	-870.6 (-1169 to -572.1)	-5.581 (-261.2 to 250.0)	198.3 (63.87 to 332.7)	2.335 (-180.7 to 185.4)
Best-fit B2 (95% CI)	-3.614 (-33.33 to 26.10)	19.71 (12.58 to 26.85)	-0.7762 (-6.885 to 5.333)	-4.317 (-7.530 to -1.104)	-0.006003 (-4.382 to 4.370)
R^2	0.01882	0.8624	0.8486	0.8167	0.04804

Where B0, B1, and B2 are parameters of the second order polynomial equation: $Y = B0 + B1*X + B2*X^2$

Table S4. Select Reactome 2022 Terms: Upregulated in CD4/CD8-selected vs. unselected ENG-T

Term	Overlap	P-value	Adjusted P-value	Odds Ratio	Combined Score	Genes
LGI-ADAM Interactions R-HSA-5682910	2/14	0.009	0.589	16.3	77.5	LGI4; ADAM11
Constitutive Signaling By NOTCH1 HD Domain Mutants R-HSA-2691232	2/15	0.010	0.589	15.1	69.4	NEURL1B; MIB2
Ion Transport By P-type ATPases R-HSA-936837	2/53	0.014	0.232	12.0	51.5	FXYD7; ATP2C2
Biological Oxidations R-HSA-211859	4/218	0.010	0.357	5.0	23.2	GSTM2; EPHX1; DPEP2; PAPSS2
RUNX3 Regulates WNT Signaling R-HSA-8951430	1/8	0.030	0.357	37.4	130.8	TCF7L2
Transport Of Vitamins, Nucleosides, And Related Molecules R-HSA-425397	2/43	0.002	0.154	30.4	182.9	SLC35D2; SLC29A4
TP53 Regulates Transcription Of Cell Death Genes R-HSA-5633008	2/44	0.003	0.154	29.6	177.2	BCL6; TP53INP1

Table S5. Select Reactome 2022 Terms: Downregulated in CD4/CD8-selected vs. unselected ENG-T

Term	Overlap	P-value	Adjusted P-value	Odds Ratio	Combined Score	Genes
Interleukin-10 Signaling R-HSA-6783783	4/45	0.000	0.038	19.4	181.1	CCR1; CCL22; CD80; LIF
Chemokine Receptors Bind Chemokines R-HSA-380108	4/56	0.000	0.044	15.3	129.6	CCR1; CXCL9; CCL22; CXCR1
Signaling By Interleukins R-HSA-449147	9/453	0.001	0.086	4.2	30.8	LYN; CCR1; CDKN1A; ITGAM; CCL22; ANXA2; IFNG; CD80; LIF
Interleukin-4 And Interleukin-13 Signaling R-HSA-6785807	4/107	0.002	0.195	7.7	46.5	CDKN1A; ITGAM; CCL22; LIF
Glycosphingolipid Metabolism R-HSA-1660662	2/45	0.005	0.178	21.5	115.9	B3GALNT1; ARSB
GPCR Downstream Signaling R-HSA-388396	5/619	0.012	0.178	3.9	17.3	CXCL9; CXCR1; TRPC3; RGS16; RGS6
Cell Cycle R-HSA-1640170	9/654	0.000	0.040	5.4	48.7	LYN; GINS2; FEN1; CDKN1A; CENPW; MCM10; CLSPN; POLR2L; SPC25
Cytokine Signaling In Immune System R-HSA-1280215	8/702	0.001	0.076	4.4	30.0	LYN; CCR1; CDKN1A; CCL22; CD40LG; ANXA2; IFNG; LIF
RNA Polymerase III Chain Elongation R-HSA-73780	2/17	0.001	0.076	46.6	316.2	POLR3K;POLR2L
Pyroptosis R-HSA-5620971	2/26	0.003	0.094	29.1	172.7	GZMB;CYCS

Table S6. Select GO Biological Processes 2023: Upregulated in CD4/CD8-selected vs. unselected ENG-T

Term	Overlap	P-value	Adjusted P-value	Odds Ratio	Combined Score	Genes
Positive Regulation Of Synaptic Transmission (GO:0050806)	5/77	0.001	0.187	6.9	46.6	NLGN2; DLG4; NOL3; BAIAP3; NFATC4
Release Of Sequestered Calcium Ion Into Cytosol By Sarcoplasmic Reticulum (GO:0014808)	2/6	0.002	0.187	49.0	318.2	RYR1; NOL3
Calcium Ion Transmembrane Import Into Cytosol (GO:0097553)	5/83	0.002	0.187	6.4	40.9	RYR1; CACNA1I; JPH2; PLCH2; CACNA1F
Regulation Of Sodium Ion Transmembrane Transporter Activity (GO:2000649)	2/37	0.007	0.278	17.5	87.2	FXYD7; FGF11
Lipid Modification (GO:0030258)	2/42	0.009	0.278	15.3	72.5	PLPPR2; EPHX2
Negative Regulation Of Lipid Kinase Activity (GO:0090219)	1/7	0.023	0.278	50.3	189.3	PIK3IP1
T-helper 17 Cell Lineage Commitment (GO:0072540)	1/7	0.023	0.278	50.3	189.3	LY9
Unsaturated Fatty Acid Metabolic Process (GO:0033559)	2/49	0.015	0.282	11.3	47.1	GSTM2; EPHX1
Icosanoid Metabolic Process (GO:0006690)	2/52	0.017	0.282	10.6	43.1	EPHX1; DPEP2
Purine Ribonucleotide Biosynthetic Process (GO:0009152)	2/55	0.019	0.282	10.0	39.6	ADCY4; PAPSS2
Positive Regulation Of Lipid Localization (GO:1905954)	2/10	0.000	0.019	208.0	1,982.0	LRP1; HILPDA
Calcium Ion Transmembrane Import Into Cytosol (GO:0097553)	3/83	0.000	0.022	32.4	282.1	RYR1; CACNA1I; JPH2
Monoatomic Cation Homeostasis (GO:0055080)	2/77	0.004	0.088	22.1	119.6	JPH2; TMPRSS6
Regulation Of Metallopeptidase Activity (GO:1905048)	1/6	0.008	0.088	159.8	775.9	LRP1
Lymphocyte Apoptotic Process (GO:0070227)	1/7	0.009	0.088	133.1	626.1	EBF4

Table S7. Select GO Biological Processes 2023: Downregulated in CD4/CD8-selected vs. unselected ENG-T

Term	Overlap	P-value	Adjusted P-value	Odds Ratio	Combined Score	Genes
Positive Regulation Of Peptidyl-Tyrosine Phosphorylation (GO:0050731)	6/130	0.000	0.064	9.8	94.8	LYN; IFNG; CD80; LIF; OSM; LRP8
Lymphocyte Proliferation (GO:0046651)	3/38	0.001	0.111	16.9	116.3	CD40LG;CTPS1;MS4A1
B Cell Receptor Signaling Pathway (GO:0050853)	3/46	0.000	0.058	33.1	291.0	IGHG2; IGHA1; MS4A1
Regulation Of T Cell Mediated Immunity (GO:0002709)	2/11	0.000	0.058	103.1	847.5	FUT7; CD80

Table S8. Surface marker phenotype of primary AML samples reported by the Johns Hopkins Hospital clinical hematopathology lab

6675	CD38, variable HLA-DR, CD117, CD123, dim CD11b, CD64, bright CD33 and bright CD13 and completely lack CD34, and are negative for CD19, CD7, CD3 and other T cell markers
6034	bright CD13 and CD34, moderate CD38, CD117, CD123 and HLA-DR with partial CD2, CD4, CD7, CD64 and CD200. There is substantial loss of CD33
5800	express CD34, partial variable CD117, CD38, partial dim CD123, bright CD13, variable CD33, and partial CD64, and with partial loss of HLA-DR
4293	Intermediate intensity CD45, negative for CD34, with expression of CD117 (dim), CD123 (dim), HLADR, CD64, CD33, and CD4. Partial dim CD7, CD15, and CD56.
4316	Variable CD34 with expression of CD117, HLADR, CD13, CD33, and CD123 and loss of CD38

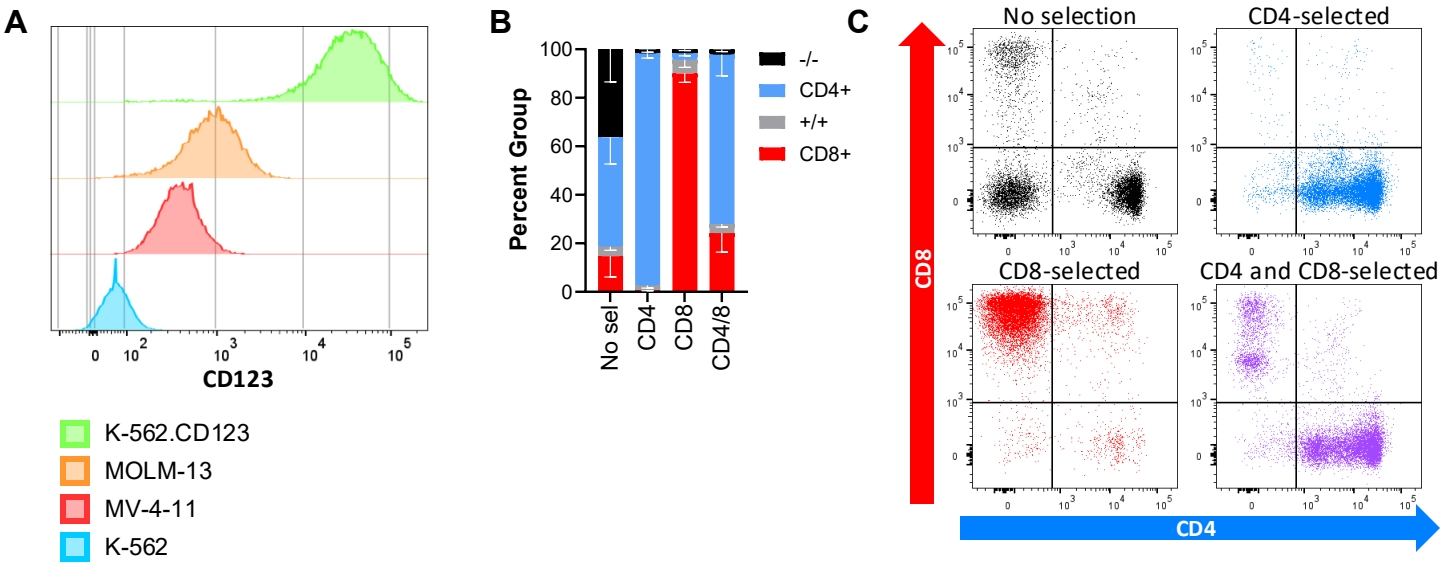

Figure S1. CD123 expression varies between model cell lines and PBMC T-cell selections result in pure populations. (A) Representative anti-CD123 antibody staining of K-562, MOLM-13, MV-4-11, and K-562 engineered to express CD123 (K-562.CD123). **(B)** Quantification of CD4+ and CD8+ population distributions following selection before activation on day 0. N = 4-6 unique T-cell donors. **(C)** Representative flow plots of selections from one donor.

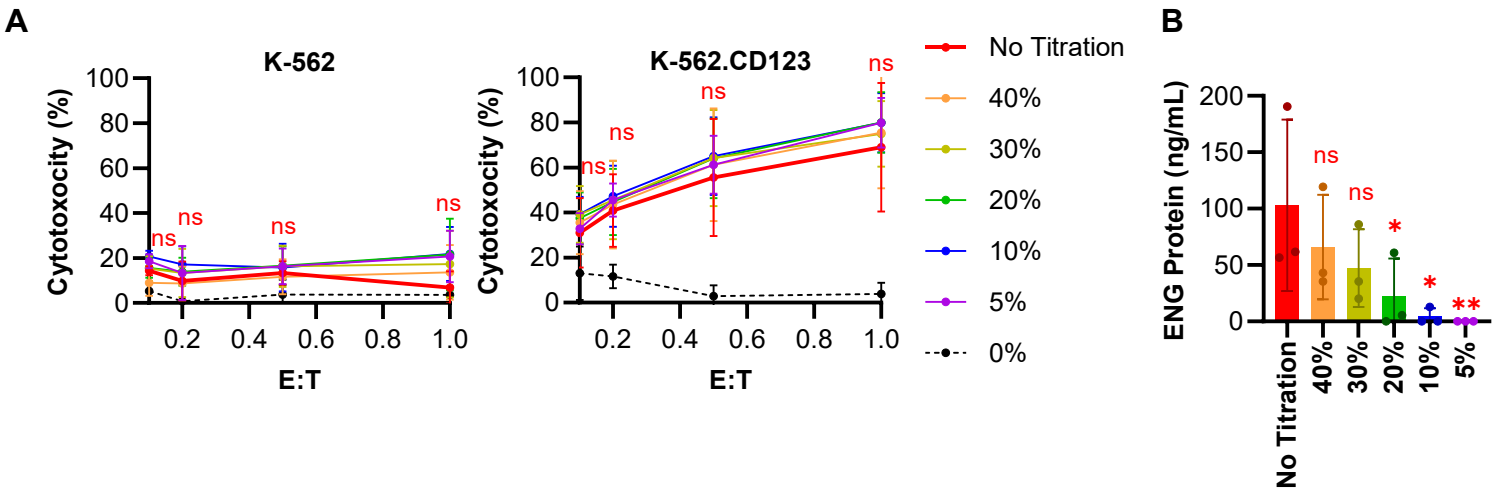

Figure S2. Antigen-specific anti-tumor activity is independent of transduction efficiency. (A) Transduced CD4/CD8-selected T cells were titrated with identically cultured autologous unmodified CD4/CD8-selected T cells to achieve the desired ENG% (0 to 64%). T cells were co-cultured with either K-562 (CD123-negative) or K-562.CD123, both engineered to express firefly luciferase, for 18-hours at indicated effector-to-target (E:T) ratios. Cytotoxicity was determined by calculating the reduction in bioluminescent signal compared to target cells cultured without T cells. Differences between selection groups at each E:T were assessed by three-way ANOVA (donor, transduction efficiency, E:T) with Tukey tests for multiple comparisons using R. N = 3 independent experiments, 2 unique T-cell donors. **(B)** CD123xCD3 secreted by 1e6 titrated cells plated in 2 mL of cytokine supplemented media measured after 24 hours by ELISA. Two-way ANOVA (donor and transduction efficiency) with Tukey correction was used to compare secreted protein amounts to no titration condition. N = 3 unique T-cell donors. For both **(A)** and **(B)**, titrated cells were allowed to incubate in cytokine-supplemented media after mixing for at least 24 hours before use in experiments. ns = not significant vs. No Titration, *$p < 0.05$, **$p \leq 0.01$. Transduction efficiency ranged from 55 to 64% in the No Titration condition.

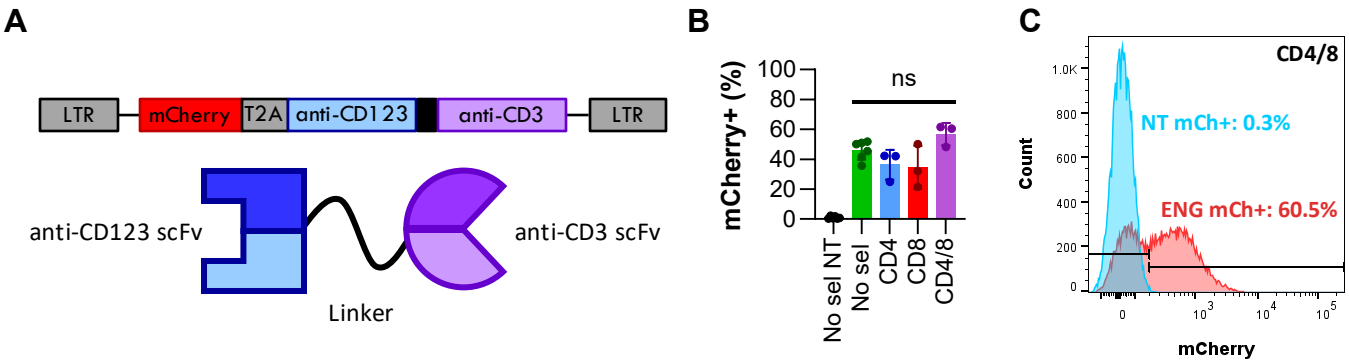

Figure S3. T cells are effectively modified with a NLS-mCherry tagged ENG construct. (A) ENG-T cells were modified with viral vectors containing mCherry tagged with a nuclear localization sequence (NLS-mCherry) and our CD123xCD3 bispecific separated by a T2A sequence. **(B)** Transduction efficiency was evaluated by flow cytometry and detection of mCherry. Two-way ANOVA (donor and selection) with Tukey correction was used to compare transduction efficiency. N = 3-6 unique T-cell donors. **(C)** Representative histogram of mCherry (mCh) positivity after transduction of CD4/8 pre-selected T cells. No sel = no selection, NT = non-transduced, CD4/8 = CD4 and CD8-selected.

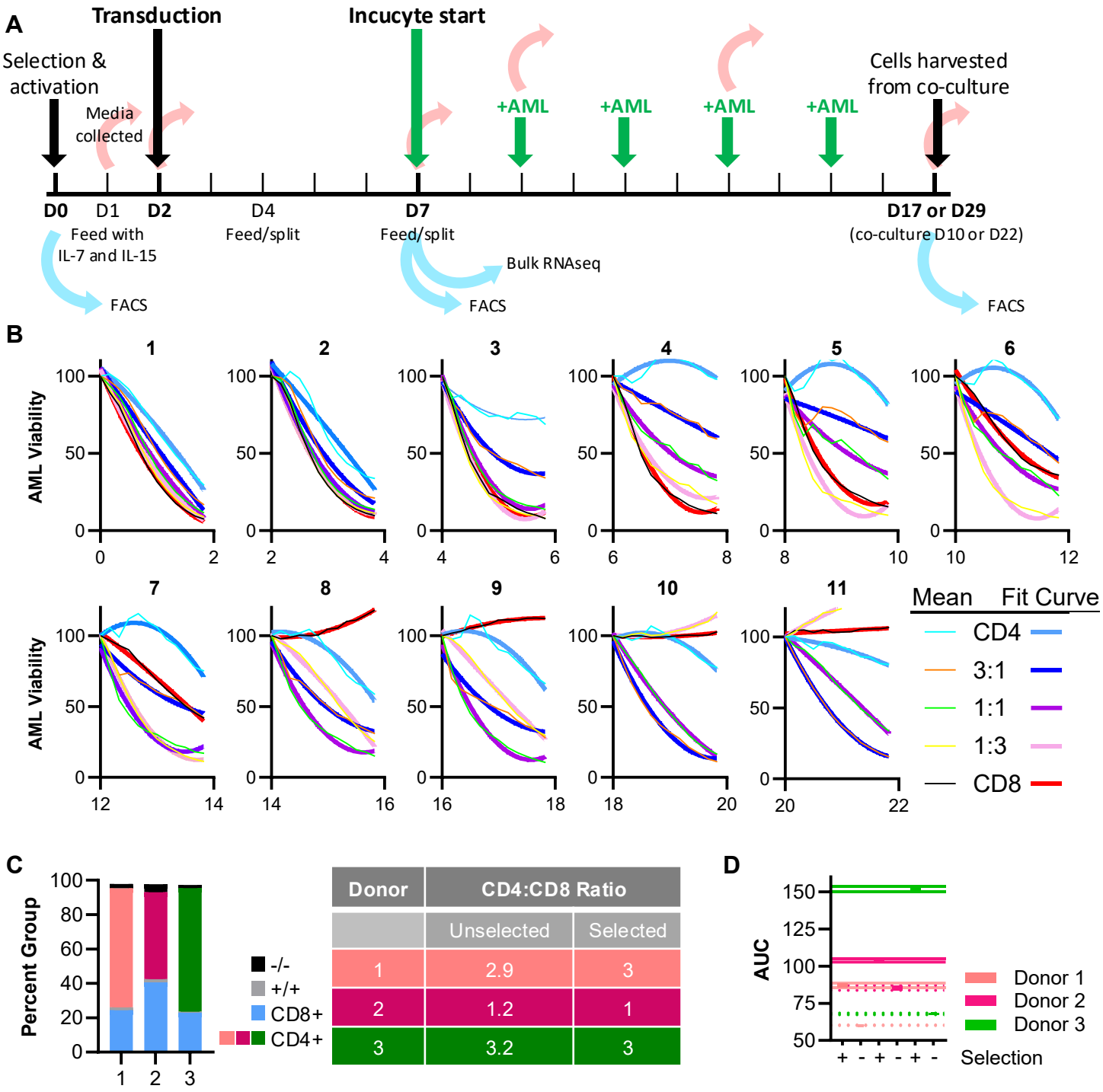

Figure S4. Pre-selection and higher CD4:CD8 ratio improve durable ENG-T cell function. (A) Experimental timeline and analytic schematic for serial stimulation, media harvest, FACS time points, and bulk RNAseq completed during manufacture and co-culture of ENG.NLSmCh-T cells with MOLM-13.NLSGFP. Cells were tracked in a 10- or 22-day serial stimulation assay (day 7 to 17 or 29 post-activation), with fresh target cells added every two days. **(B)** AML viability is calculated as the average number of green objects counted per image, as a percentage of the total number of green objects recorded at the initiation of each stimulation. AML viability recorded over 11 stimulations and 22 total days in culture with ENG-T cell products with variable CD4:CD8 ratios, as indicated. AML viability curve comparisons were visualized by fitting quadratic curves to each stimulation. 4 images per well, 3 wells per donor and 3 unique T cell donors measured per condition. **(C)** T-cell composition of unselected ENG-T cell products per donor. **(D)** Area under the curve (AUC) calculated for T-cell counts and depicted as 95% confidence interval bound for each condition. Dotted: no selection, Solid: Selection.

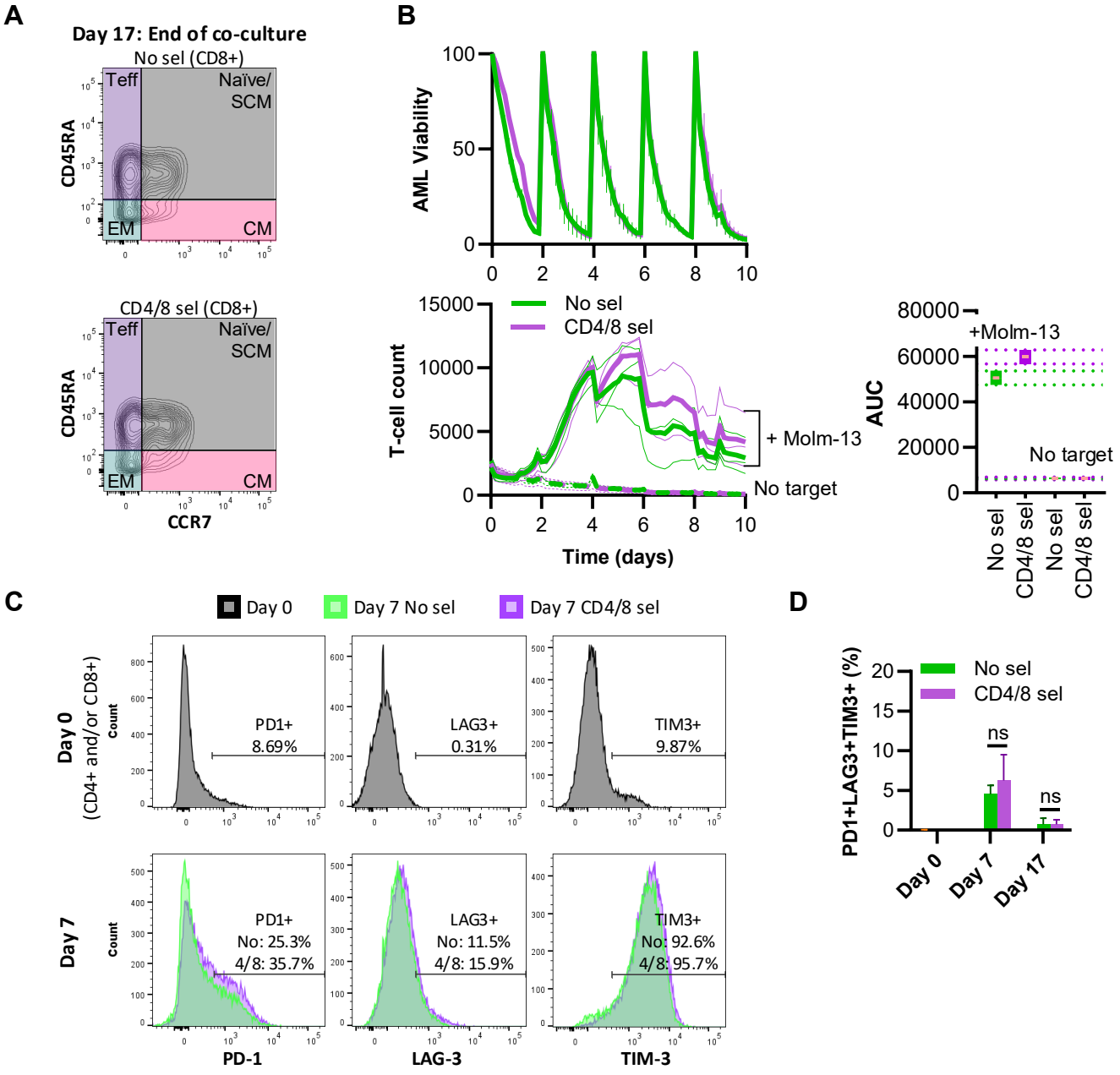

Figure S5. Unselected and CD4/CD8-selected ENG-T cells functional differences not explained by differential expression of exhaustion associated receptors. (A) Representative flow cytometry plots used to define T-cell immunophenotypic subsets of unselected and CD4/CD8-selected ENG.NLSmCh-T cells. **(B)** ENG-T cells and MOLM-13 marked with NLS-mCherry and NLS-GFP, respectively were co-cultured in an Incucyte S3 live cell imaging system at an initial effector-to-target ratio of 1:1 per well. Cells were tracked in a 10-day serial stimulation assay (day 7 to 17 post-activation), with fresh target cells added every two days. T cells per image were quantified (thick lines = means, thin lines = individual donors) and cytotoxicity was determined by measurement of target cells per image. AML viability is represented as the average number of green objects counted per image, as a percentage of the total number of green objects recorded after re-stimulation. T-cell count is representative of the average number of red objects counted per image. 4 images per well, 6 wells per donor, 3 independent T-cell donors. Area under the curve (AUC) calculated for T-cell counts and depicted as 95% confidence interval for each condition. **(C)** Representative flow cytometry histograms showing PD-1, LAG-3, and TIM-3 surface expression on T cells before activation on day 0 and surface expression on ENG.NLSmCh-T cells following 7 days of culture. No sel = no selection, CD4/8 = CD4 and CD8-selected. **(D)** Exhausted cell percentages were measured before and after serial stimulation (D7 vs. D17). Statistical comparison was completed using two-way ANOVA (donor and selection).

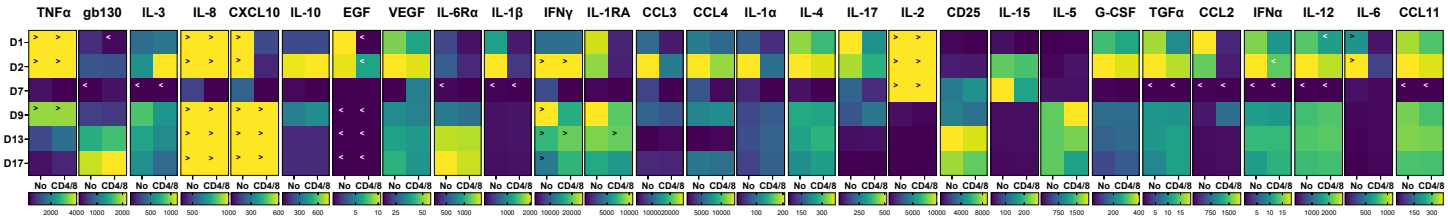

Figure S6. The manufacturing environment of unselected and selected ENG-T cells differs only in the initial days of culture. A panel of cytokines were measured in the supernatant of unselected or CD4/CD8-selected ENG.NLSmCh-T cells during manufacture (day 1, 2, and 7) and serial stimulation (day 9, 13, 17) using a Luminex multiplex assay. A greater-than sign indicates at least one sample above the limit of detection, a less-than sign indicates at least one sample below the limit of detection. Heatmap scale differs for each analyte tested and is indicated below each map. N = 3 unique T-cell donors. No sel = no selection, CD4/8 = CD4 and CD8-selected.

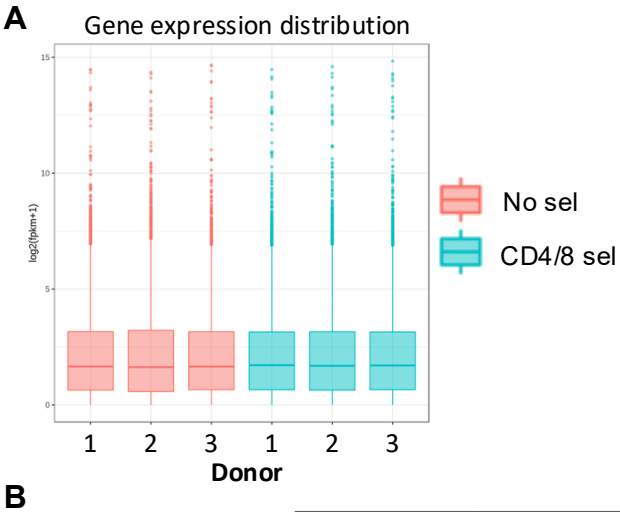

Figure S7. CD4/CD8-selection alters the transcriptional profile of ENG-T cells. RNA was extracted from unselected and CD4/CD8-selected ENG.NLSmCh-T cells frozen on day 7 of manufacture. Transcription profiles were assessed by bulk RNAseq. **(A)** Levels of total gene expression were calculated for each selection group and donor. **(B)** Clustering of ENG-T cells using $\log_2$(FPKM+1) and normalized expression of transcripts. Major groups of upregulated or downregulated transcripts are separated by orange lines and were defined by the apparent drivers of each cluster. Clusters driven by selection are also reported in **Figure 6A** and were further broken down into subcluster gene sets, indicated by dashed orange lines, for Enrichr analysis. N = 3 unique T-cell donors. No sel = no selection, CD4/8 = CD4 and CD8-selected.

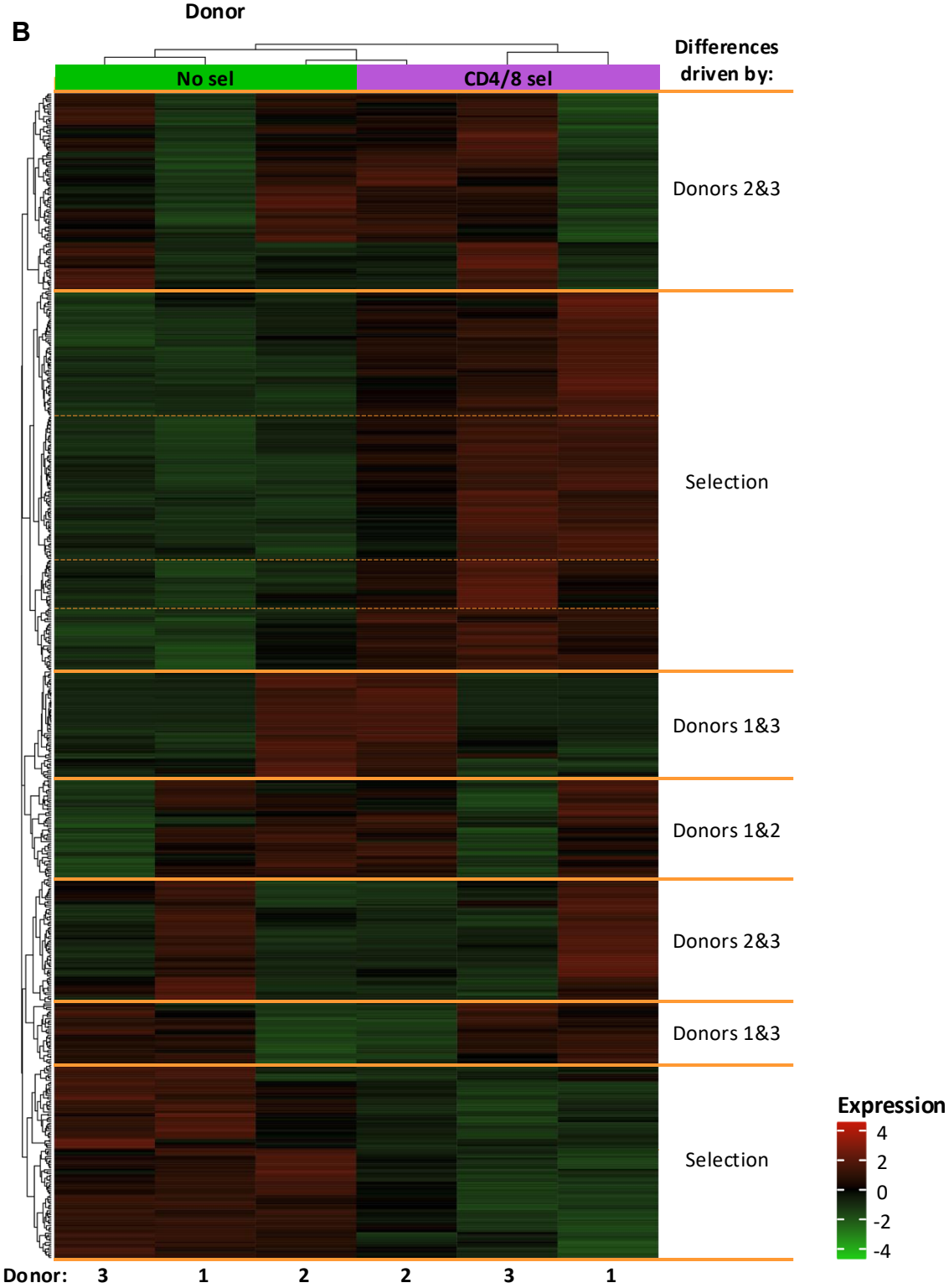

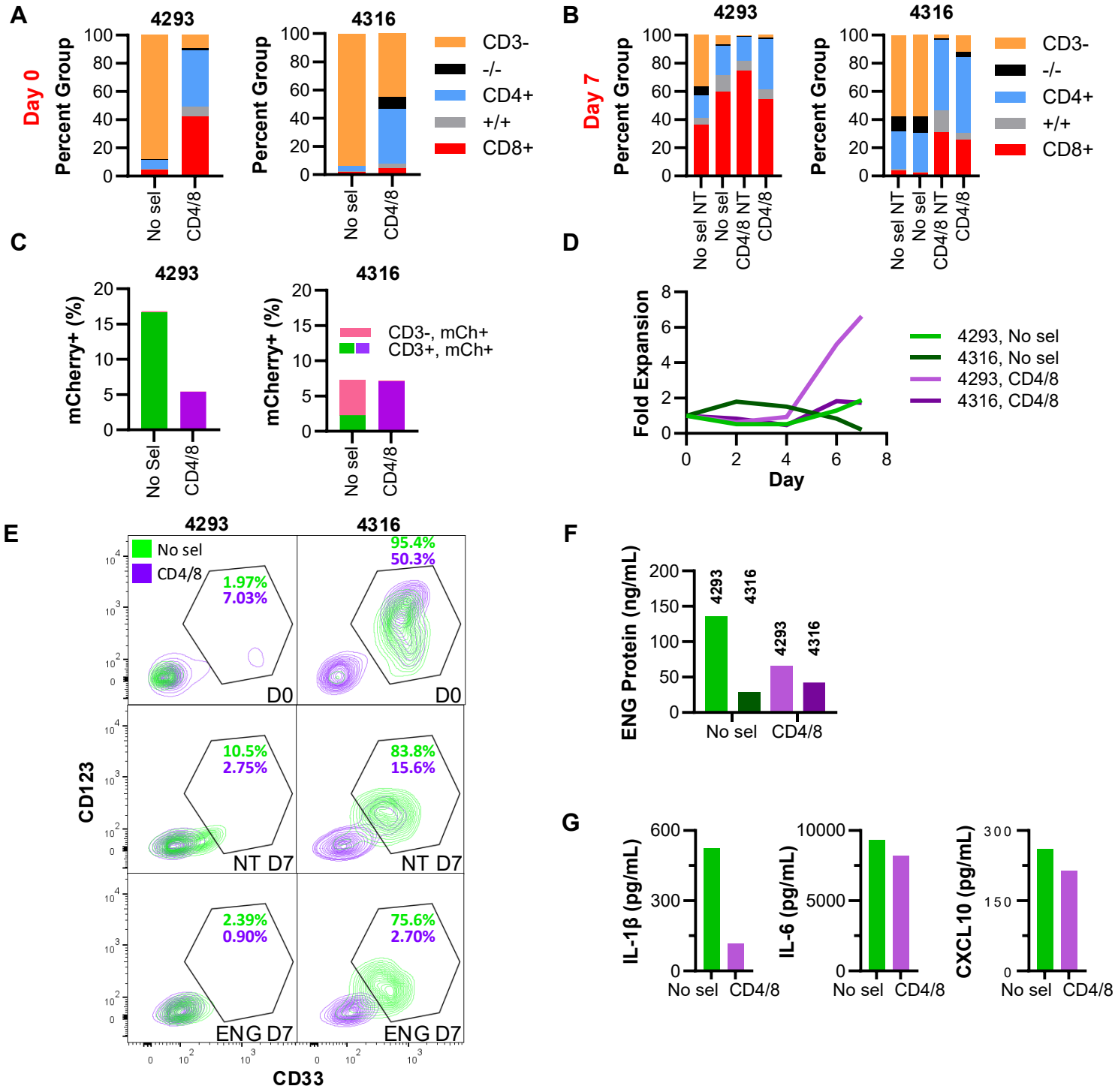

Figure S8. CD4/CD8-selected ENG-T cells produced from patient-derived material have decreased CD3-negative contamination and increased expansion. ENG-T cells were produced from banked bone marrow aspirates from two patients treated at the Johns Hopkins Hospital. **(A)** T cells from patient 4293 and patient 4316 were activated on day 0 either without or after CD4/CD8-selection. CD3+, CD4+, and CD8+ populations were detected using flow cytometry. **(B)** CD3-negative contamination was evaluated on day 7 post-activation using flow cytometry. **(C)** Unselected and selected cells were transduced with an NLS-mCherry tagged ENG vector and expression of mCherry was detected on day 6 post-activation using flow cytometry **(D)** Expansion of unselected and selected products was evaluated by manual counting. **(E)** The presence of AML (CD123+CD33+) was detected in the material used for unselected and CD4/CD8-selected ENG-T cell manufacture (day 0, D0), in non-transduced expanded T cells, and in expanded ENG-T cell products. Expanded products were evaluated on day 7 (D7) after activation. CD123 and CD33 staining was assessed by flow cytometry. **(F)** Production of CD123xCD3 was confirmed in the expansion media of transduced cell products by ELISA. **(G)** The presence of IL-1β, IL-6, and CXCL10 were detected in the T-cell expansion media of sample 4293 on the day following activation. Protein concentrations were determined by ELISA. No sel = no selection, CD4/8 = CD4 and CD8-selected.

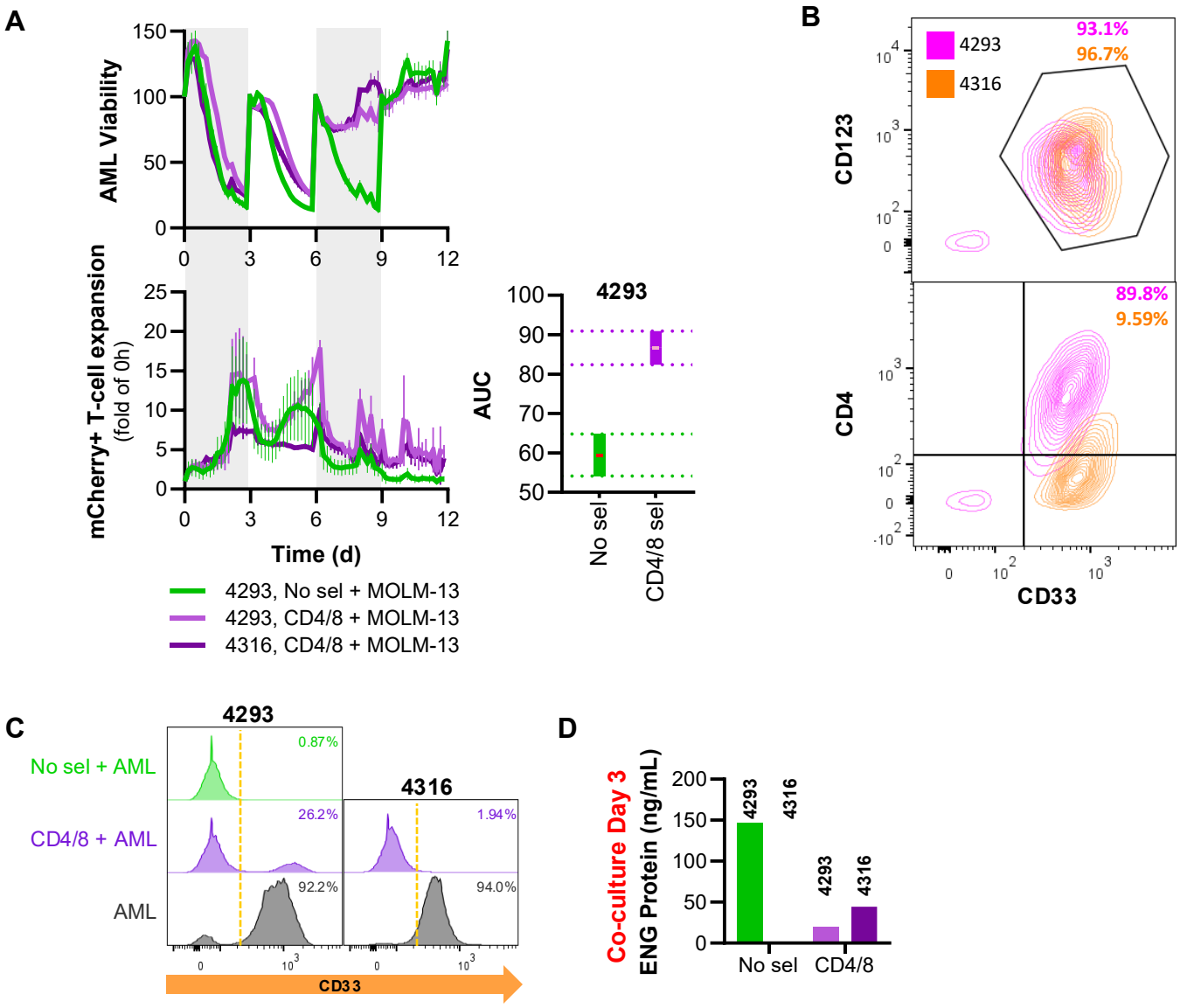

Figure S9. ENG-T cells engineered from patient samples kill AML blasts. (A) ENG-T cell products with effective expansion were plated 1:1 with MOLM-13.NLSGFP in an Incucyte S3 live cell imaging system. T cells were restimulated with more MOLM-13.NLSGFP every 3 days for 12 days (d). AML viability was calculated as the percentage of green objects remaining after each re-stimulation. T-cell expansion was tracked by evaluating the fold change of red objects compared to time 0. For each donor, 3 wells were plated and 4 images were gathered per well. 95% confidence interval for calculated Area Under the Curve (AUC) of matched donor T-cell expansion. **(B)** Expression of CD33, CD123, and CD4 in AML samples from patient 4293 and 4316, determined by flow cytometry. **(C)** ENG-T cell products were plated at a 1:1 ratio with autologous AML. Viable CD33+ cells were evaluated after 72h by flow cytometry. **(D)** The presence of CD123xCD3 molecules was detected in the media of ENG-T and autologous AML co-cultures using ELISA. No sel = no selection, CD4/8 = CD4 and CD8-selected, NT = non-transduced.